A complex of ZO-1 and the BAR-domain protein TOCA-1 regulates actin assembly at the tight junction

Christina M. Van Itallie[a], Amber Jean Tietgens[a], Evan Krystofiak[b], Bechara Kachar[b], and James M. Anderson[a]

[a]Laboratory of Tight Junction Structure and Function, National Heart, Lung, and Blood Institute, and [b]Laboratory of Cell Structure and Dynamics, National Institute of Deafness and Other Communication Disorders, National Institutes of Health, Bethesda, MD 20892

ABSTRACT **Assembly and sealing of the tight junction barrier are critically dependent on the perijunctional actin cytoskeleton, yet little is known about physical and functional links between barrier-forming proteins and actin. Here we identify a novel functional complex of the junction scaffolding protein ZO-1 and the F-BAR–domain protein TOCA-1. Using MDCK epithelial cells, we show that an alternative splice of TOCA-1 adds a PDZ-binding motif, which binds ZO-1, targeting TOCA-1 to barrier contacts. This isoform of TOCA-1 recruits the actin nucleation–promoting factor N-WASP to tight junctions. CRISPR-Cas9–mediated knockout of TOCA-1 results in increased paracellular flux and delayed recovery in a calcium switch assay. Knockout of TOCA-1 does not alter FRAP kinetics of GFP ZO-1 or occludin, but longer term (12 h) time-lapse microscopy reveals strikingly decreased tight junction membrane contact dynamics in knockout cells compared with controls. Reexpression of TOCA-1 with, but not without, the PDZ-binding motif rescues both altered flux and membrane contact dynamics. Ultrastructural analysis shows actin accumulation at the adherens junction in TOCA-1–knockout cells but unaltered freeze-fracture fibril morphology. Identification of the ZO-1/TOCA-1 complex provides novel insights into the underappreciated dependence of the barrier on the dynamic nature of cell-to-cell contacts and perijunctional actin.**

Monitoring Editor
Alpha Yap
University of Queensland

Received: Apr 20, 2015
Revised: May 27, 2015
Accepted: Jun 5, 2015

INTRODUCTION

Tight junctions form the barrier between epithelial cells that limits the paracellular movement of water and solutes across tissue layers (Shen *et al.*, 2011; Gunzel and Yu, 2013). The sealing proteins are transmembrane proteins that interact with partners on adjacent cells and include claudins, MARVEL domain–containing proteins, including occludin, and members of the junctional adhesion molecule (JAM) immunoglobulin superfamily (Furuse, 2010). All three of these protein families bind directly to the scaffolding protein ZO-1 at the tight junction; claudins and JAMs bind to PDZ domains in the N-terminal half of ZO-1 (Fanning and Anderson, 2009). ZO-1 also binds directly to perijunctional F-actin and other components of the cytoskeleton and appears well positioned to coordinate barrier function with cytoskeletal changes (Fanning and Anderson, 2009). Both the initial assembly of the junction and maintenance of the seal depend on the organization of perijunctional actin (Rodgers and Fanning, 2011). A dynamic coupling between the barrier and the cytoskeleton is presumably required since the tight junction must maintain an Ångström-level paracellular seal in the face of continuous intercellular movements, apoptosis, and epithelial restitution (Guillot and Lecuit, 2013). It remains unclear how this dynamic clutch-like coupling occurs.

To better understand which proteins might be important in barrier physiology, we recently catalogued the proteins that are proximal to ZO-1 (Van Itallie *et al.*, 2013) using BioID, a biotin ligase–based tagging proteomics method (Roux *et al.*, 2012). Surprisingly, among the most abundant proteins identified using this method

This article was published online ahead of print in MBoC in Press (http://www.molbiolcell.org/cgi/doi/10.1091/mbc.E15-04-0232) on June 10, 2015.

Address correspondence to: Christina M. Van Itallie (Christina.vanitallie@nih.gov).

Abbreviations used: CIP4, Cdc42-interacting protein 4; FBP17, formin-binding protein 17; N-WASP, neural Wiskott–Aldrich syndrome protein; TOCA-1, transducer of cdc42-dependent actin activity.

was the F-BAR–domain protein transducer of cdc42-dependent actin activity (TOCA-1; also called formin-binding protein 1-like). TOCA-1 was originally discovered in an in vitro screen designed to identify components of a Cdc42-dependent actin polymerization pathway (Ho *et al.*, 2004). In that study, Kirschner and colleagues found that TOCA-1 bound both the small GTP-binding protein Cdc42 and neural Wiskott–Aldrich syndrome protein (N-WASP; the ubiquitous form of WASP) and that it could activate the N-WASP/WASP-interacting protein (WIP) complex, the form in which WASP is normally found in cells. Activation of N-WASP/WIP then promoted branched actin nucleation by activation of the Arp2/3 complex. A subsequent study (Takano *et al.*, 2008) found that TOCA-1/WASP/WIP could stimulate actin polymerization in the absence of Cdc42 when the complex was activated by binding of the BAR domain to curved phosphatidylserine-containing membranes. These authors found that the positioning of N-WASP/WIP close to membranes was dependent on TOCA-1 and this positioning was required for actin nucleation at the membrane.

TOCA-1 is a member of a larger family of F-BAR proteins that share a membrane-binding N-terminal domain that organizes into curved dimers and higher-order multimers (Itoh *et al.*, 2005; Henne *et al.*, 2007; Shimada *et al.*, 2007; Frost *et al.*, 2008). Through cooperative assembly into curved structures, these proteins can sense and/or create membrane curvature. Like TOCA-1, several other F-BAR proteins bind N-WASP, and thus as a family they are well positioned to couple dynamic membrane events with cytoskeletal remodeling (Heath and Insall, 2008; Fricke *et al.*, 2010). Some F-BAR domain–containing proteins have been implicated in endocytosis (Leibfried *et al.*, 2008), particularly in *Drosophila* (Fricke *et al.*, 2009) and *Caenorhabditis elegans* (Giuliani *et al.*, 2009), but the importance of the mammalian TOCA-1 in this process is controversial (Tsujita *et al.*, 2006; Bu *et al.*, 2009). In contrast, there is clear evidence that TOCA-1 can play a role in regulation of cell migration in epidermal and breast tumor cells (Hu *et al.*, 2011; Chander *et al.*, 2013).

Although perijunctional actin is most conspicuous near E-cadherin–based adherens junctions, it has long been recognized that actin is also associated with tight junctions. Freeze-etch and transmission electron microscopy first demonstrated an intimate relationship between actin filaments and tight junction membrane contacts more than 30 years ago (Hirokawa and Tilney, 1982; Hirokawa *et al.*, 1983; Madara *et al.*, 1987). Similarly, pharmacologic disruption of actin organization with cytochalasin D results in disorganization of tight junction strands (Bentzel *et al.*, 1980; Madara *et al.*, 1986), which coincides with increased paracellular permeability (Ma *et al.*, 1995). It was demonstrated that the ZO proteins (homologues ZO-1, -2, and -3) and the tight junction protein cingulin bind directly to actin and that ZO proteins also bind many actin-regulatory proteins, including cingulin, protein 4.1, AF-6/afadin, cortactin, α-actinin 4, and myosin 1C (Fanning *et al.*, 1998; Cordenonsi *et al.*, 1999; Mattagajasingh *et al.*, 2000; Chen *et al.*, 2006; Ooshio *et al.*, 2010; Goldblum *et al.*, 2011; Kremerskothen *et al.*, 2011). ZO-1 is also known to interact with regulators of myosin II activity such as Shroom2 and MRCKβ (Etournay *et al.*, 2007; Huo *et al.*, 2011) and regulators of Rho GTPase signaling such as the Cdc42GEF Tuba and paracingulin (Otani *et al.*, 2006; Pulimeno *et al.*, 2011; reviewed by Rodgers and Fanning (2011)). However, despite this sizable inventory of interacting proteins, it is unclear how ZO-1 is involved in actin regulation at the tight junction. The goal of the present study was to determine whether the actin regulatory protein TOCA-1 might play a critical functional role in actin organization at the tight junction.

RESULTS

TOCA-1 partially colocalizes with ZO-1 at epithelial tight junctions

A BioID (Roux *et al.*, 2012) screen using biotin ligase fused to ZO-1 unexpectedly identified TOCA-1 as among the most abundant proteins proximal to ZO-1 (Van Itallie *et al.*, 2013). Confocal imaging in Madin–Darby canine kidney (MDCK; Figure 1A, top row) and Caco-2 (Figure 1B, middle row) cells revealed clear junctional TOCA-1 immunofluorescence (Figure 1A, middle column) that overlapped with ZO-1 (Figure 1A, left column and merge, right column), although cytoplasmic staining of TOCA-1 was also evident. Verifying the in vivo relevance, TOCA-1 was also observed concentrated with ZO-1 in tissue sections from mouse kidney (Figure 1A, bottom row). Structured illumination microscopy (SIM) was used to better resolve the position of TOCA-1 relative to ZO-1, E-cadherin, actin, and myosin (Figure 1B). Using ZO-1 immunofluorescence to define the location of the tight junction (Figure 1B, top left), some TOCA-1 was found precisely colocalized with ZO-1 at cell contacts (Figure 1B, top middle and merge). In contrast, both perijunctional actin (Figure 1B, middle row, left) and nonmuscle myosin 2B (Figure 1B, bottom row) were found near but not coincident with TOCA-1. The distribution of actin partially overlapped with TOCA-1, but some junctional actin appeared to be slightly farther from the membrane contacts (Figure 1B, second row, middle and merge). In contrast, myosin 2B was concentrated in puncta that paralleled but did not overlap with TOCA-1 (Figure 1B, bottom row, middle and merge). These results show that TOCA-1 and ZO-1 colocalize and are positioned closer to the membrane than the majority of the actin and myo2B.

TOCA-1 is targeted to the tight junction by an alternatively spliced PDZ-binding motif at its C-terminus

All reported TOCA-1 sequences included F-BAR, HR1, and SH3 domains (Figure 2A, top), but reported isoforms include several splice variants. Published studies of TOCA-1 used the canonical sequence (Uniprot isoform 1, Q5T0N5-1; Figure 2A, middle) and the shorter published cDNA for TOCA-1 (Ho *et al.*, 2004; isoform 3, Q5T0N5-3). We noted that two other TOCA-1 isoforms were predicted in databases (Uniprot isoforms 4, Q5T0N5-4, and 5, Q5T0N5-5) and ended in a C-terminal splice with an amino acid sequence matching the consensus for a canonical type I PDZ-binding motif, S/T-X-I/V (Figure 2A, bottom; Songyang *et al.*, 1997). This type of PDZ-binding motif is characteristic of the tails of claudins known to interact with the first of the three PDZ domains of ZO-1, -2, and -3. Quantitative real-time PCR (qRT-PCR) amplification of cDNA made from MDCK cells, Caco-2 cells, primary human dermal fibroblasts, and the fibroblastic cell line HEK 293 cells demonstrated the presence of both isoforms in all cell lines. However, relative to ZO-1 expression levels, the transcript for the isoform(s) containing the putative PDZ-binding motif, TOCA-1(+), was expressed at >20-fold higher levels than the transcript for isoform(s) lacking the PDZ-binding motif, TOCA-1(–), in MDCK cells and at fivefold higher levels in Caco-2 cells. In contrast, expression of transcripts for both isoforms was much lower and that of both isoforms nearly equal in the fibroblastic cell lines. These results suggest that expression of TOCA-1(+) may be a special feature of epithelial cells.

ZO-1 is required for the localization of TOCA-1 at cell contacts, since in Caco-2 cells depleted of ZO-1 using small interfering RNAs (siRNAs), there was a dramatic reduction in TOCA-1 at cell contacts (Figure 2C). As a control, TOCA-1 was colocalized with ZO-1 in cells transfected with a nontargeting siRNA (Figure 2C, top). Transfection with an siRNA targeting ZO-1 resulted in a mosaic of normal and ZO-1–depleted cells. In islands of cells in which ZO-1 expression

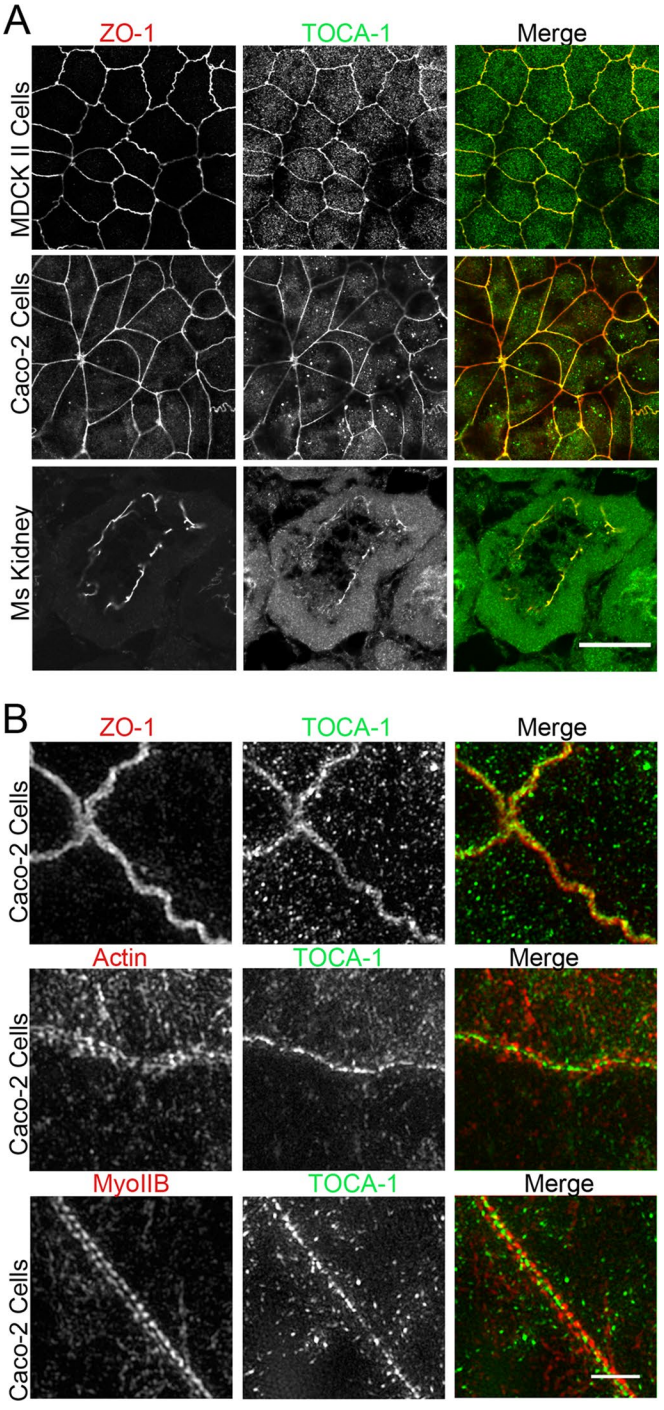

FIGURE 1: TOCA-1 partially colocalizes with ZO-1 at the tight junction. (A) Confocal immunofluorescence analysis reveals partial colocalization of ZO-1 (left) with TOCA-1 (middle) in the merged images (right) in MDCK II cells (top), Caco-2 cells (middle), and mouse kidney tubules (bottom). Bar, 20 μm. (B) Superresolution microscopy confirms that a component of immunoreactive TOCA-1 colocalizes with ZO-1. Full depth projection immunofluorescence localization of ZO-1 and TOCA-1 (top) in Caco-2 cells as detected using structured illumination microscopy confirmed their colocalization at tight junctions. Middle, actin and TOCA-1 immunofluorescence colocalization reveals that much junctional actin lies farther from the cell membrane relative to the TOCA-1 signal. Bottom, similarly, Myo2B immunofluorescence is evident on either side of the tight junction but does not colocalize with TOCA-1. Bar, 2 μm.

was present (Figure 2C, top half of bottom images), TOCA-1 was junctional, whereas in areas where ZO-1 expression was depleted, there was little junctional TOCA-1 (Figure 2C, bottom half of bottom images). Similarly, staining for TOCA-1 at tight junctions was markedly decreased in ZO-1/ZO2 double-knockdown cells (Supplemental Figure S1; Fanning *et al.*, 2012).

To test whether the PDZ-binding motif was required to localize TOCA-1 to the tight junction, we expressed N-terminally green fluorescent protein (GFP)–tagged constructs of TOCA-1 with (+) and without (–) the putative PDZ-binding motif transiently in MDCK cells. Fluorescently tagged TOCA-1(–) was diffusely localized (Figure 2D, top row), whereas some TOCA-1(+) specifically colocalized with ZO-1 at cell contacts (Figure 2D, bottom row). ZO-1 contains three PDZ domains in its N-terminal region; to determine whether these domains were responsible for the interaction with TOCA-1, we expressed GFP alone and GFP-tagged TOCA-1 with and without the PDZ-binding motif in HEK 293T cells and immobilized the expressed fusion proteins on GFP-Trap resin. The resin with bound protein was mixed with lysate from HEK cells expressing myc-tagged ZO-1 (the N-terminal 1–887 residues) and myc-tagged ZO-1 deletion mutants lacking the first, second, or third PDZ domains. Immunoblot analysis of bound ZO-1 proteins (Figure 2, E, quantified in F) demonstrated that the most robust interaction of TOCA-1(+) was with the full N-terminal half of ZO-1 and with a construct lacking the third PDZ domain. Deletion of PDZ1 resulted in almost complete loss of interaction between the two proteins, consistent with its behavior as a type I PDZ-binding interaction (Songyang *et al.*, 1997). However, deletion of the second PDZ domain also decreased binding between TOCA-1(+) and ZO-1; this is similar to a recent report that the presence of ZO-1 PDZ2 is also required for its interaction with claudin- 2 (Rodgers *et al.*, 2013). The contribution of PDZ2 could be due to a non–PDZ-dependent interaction with TOCA-1(+) or, based on similar results with claudin-2, may reflect a requirement for ZO dimerization through PDZ2 (Rodgers *et al.*, 2013) in modulating the efficiency of TOCA-1(+) binding to the first PDZ domain.

Clustered regularly interspaced short palindromic repeat/Cas9 knockout of TOCA-1 does not alter levels or localization of tight or adherens junction proteins

To determine a possible functional role for TOCA-1 in tight junction assembly and physiology, we made clustered regularly interspaced short palindromic repeat (CRISPR)–mediated knockouts of TOCA-1 in MDCK cells. Exon organization of the TOCA-1 gene made it impossible to target only the PDZ-binding motif area without affecting the SH3-binding domain, so we instead created global TOCA-1 knockouts. Constructs were designed to target sequences in exon 3; after transfection, selection, and dilution cloning to single cells, we tested expanded clonal lines for expression of TOCA-1 by immunoblots. Genomic DNA in the region of the targeted sequences from several negative clones was amplified by PCR and sequenced. Comparison of knockout with wild-type DNA sequence (Figure 3A) showed a 5–base pair deletion in the knockout cells, resulting in a frameshift in amino acid sequence producing a stop codon at TOCA-1 amino acid residue 36. In control cells, as shown previously, TOCA-1 staining partially colocalized with ZO-1 staining (Figure 3, B, top, and higher-magnification image, C). In contrast, immunofluorescence analysis of TOCA-1–knockout cells showed only background fluorescence in the knockout cells (Figure 3B, middle bottom, compared with middle top); ZO-1 localization was unaffected. Colocalization of TOCA-1 with E-cadherin in control MDCK cells (Figure 3, D, top rows, and higher-magnification image, E) revealed

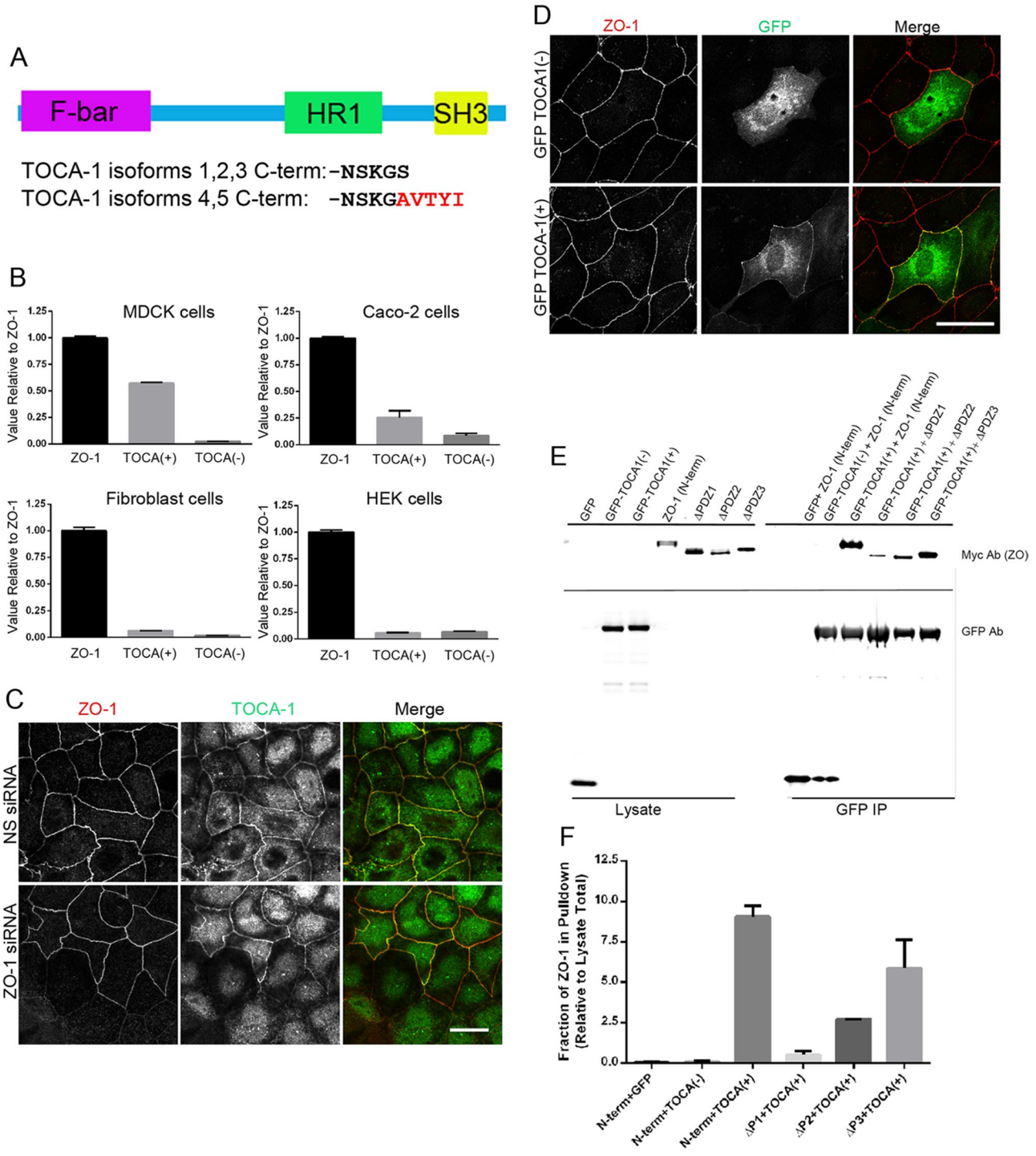

FIGURE 2: A splice form of TOCA-1 terminates in a PDZ-binding motif, which interacts with the first PDZ domain of ZO-1 and targets it to tight junctions. (A) Top, diagram of conserved function domains in TOCA-1 including the F-bar domain, HR1 (Rho/Cdc42 binding) domain, and SH3 domain. Middle and bottom, two splice forms of human TOCA-1 differ in their C-terminal sequences; one (present in isoforms 4 and 5) contains a putative PDZ-binding motif (in red). (B) qRT-PCR demonstrates that transcripts for the splice form containing the PDZ-binding motif was expressed at threefold to fivefold higher levels than that lacking the PDZ-binding motif in both epithelial cells lines, whereas expression of either TOCA-1 with or without the putative PDZ-binding motif was present at much lower levels in a primary fibroblast cell line or in the transformed fibroblastic HEK cells. (C) siRNA-mediated knockdown of ZO-1 in Caco-2 cells demonstrates a requirement for ZO-1 in localization of TOCA-1 to tight junctions. In cells transfected with a nonspecific (NS) siRNA (top), ZO-1 and TOCA-1 localization is similar to control cells. In cells transfected with an siRNA targeting ZO-1 (bottom), patches of knockdown cells showed diminished ZO-1 staining and similarly decreased junctional TOCA-1 immunofluorescence. Bar, 15 μm. (D) Transient expression of fluorescently tagged (GFP) TOCA-1(–) in MDCK cells (top) failed to localize at cell contacts with ZO-1 and was distributed diffusely within cells. In contrast (bottom), transient expression of GFP TOCA-1(+) in MDCK cells colocalized with ZO-1 at tight junctions. Bar, 10 μm. (E) In vitro

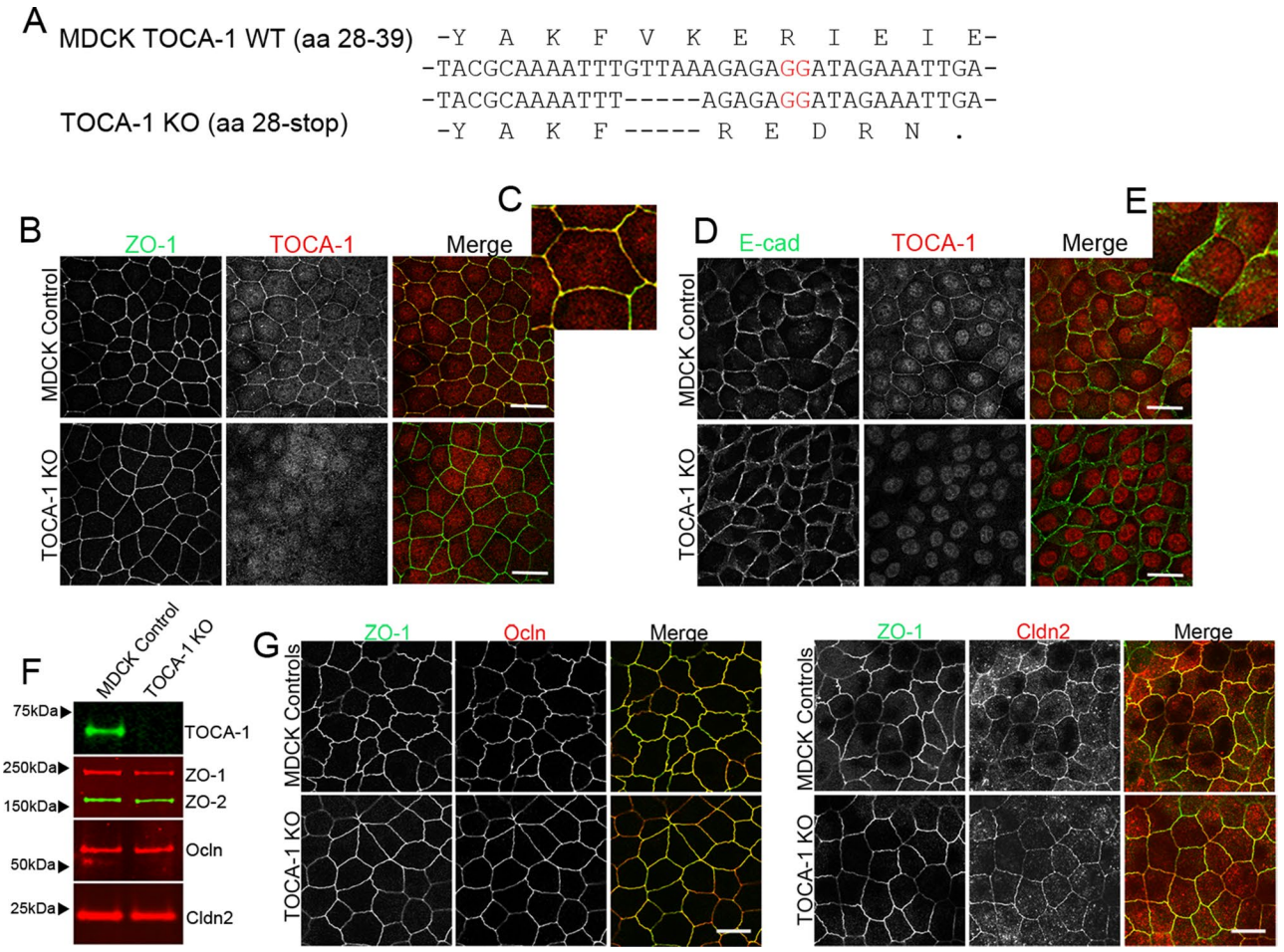

FIGURE 3: CRISPR-mediated knockout of TOCA-1 does not alter levels or localization of tight or adherens junction proteins. (A) Sequencing of PCR products amplified from genomic MDCK cell DNA in a region around the site of the putative CRISPR-mediated showed knockout cells had a 5–base pair deletion upstream of the PAM site (red GG) relative to wild-type DNA, resulting in a frameshift in the coding sequence and a premature stop codon at amino acid 36. (B) Comparison of expression by immunofluorescence analysis demonstrates that ZO-1 signal is identical in control and knockout cells (left and right). Junctional TOCA-1 staining is evident only in control cells, although the polyclonal TOCA-1 antibody generates some background signal in knockout cells (middle). (C) Enlargement of control ZO-1 and TOCA-1 staining reveals strong junctional colocalization (yellow signal). (D) E-cadherin (Ecad) localization is similar in control (top) and knockout cell lines (bottom). (E) In contrast to clear colocalization of TOCA-1 with ZO-1, enlargement of merge image between E-cadherin and TOCA-1 reveals that most E-cadherin is distributed along the lateral membrane, with little of the yellow signal suggestive of colocalization that is evident in C. Immunoblot (F) and immunofluorescence (G) analyses used to compare expression and localization of TOCA-1 and tight junction proteins in control and TOCA-1–knockout cell lines. Cldn2, claudin-2; Ocln, occludin. Bar, 15 μm.

only weak colocalization, with the abundant E-cadherin staining along the lateral cell membrane. TOCA-1 knockout had no apparent effect on E-cadherin distribution (Figure 3D, bottom row).

Immunoblot (Figure 3F) and immunofluorescence (Figure 3G) analysis of other tight junction proteins, including ZO-1, occludin, and claudin-2, showed that TOCA-1 knockout affected neither their levels nor their distribution. Similarly, levels (Supplemental Figure S2) and distribution (Supplemental Figure S2) of several adherens junction proteins were unchanged in the TOCA-knockout cells compared with control cells. In addition, freeze-fracture electron microscopy of control and knockout cells (Figure 4) showed no obvious differences in pattern or number of tight junction fibrils. In summary,

binding assays demonstrate that TOCA-1(+) primarily interacts with the first PDZ domain of ZO-1. Lysates from HEK cells expressing GFP, GFP TOCA-1(–), and GFP TOCA-1(+) were bound to GFP-Trap resin and washed, and resin was then mixed with lysate from HEK cells expressing the Myc-tagged N-terminal half of ZO-1 and the same construct lacking the first (ΔPDZ1), second (ΔPDZ2), or third (ΔPDZ3) PDZ-binding motif. Beads were washed and bound protein eluted with SDS–PAGE sample buffer. Top, samples immunoblotted for the Myc tag; bottom, immunoblotted with anti-GFP antibody; left, lysates; right, bound proteins. (F) Quantification of the amount of ZO-1 pulled down in two similar experiments as in D reveals PDZ-binding motif–dependent interaction of myc-tagged ZO-1 to GFP TOCA-1(+) and that PDZ1 is required for TOCA-1(+) binding.

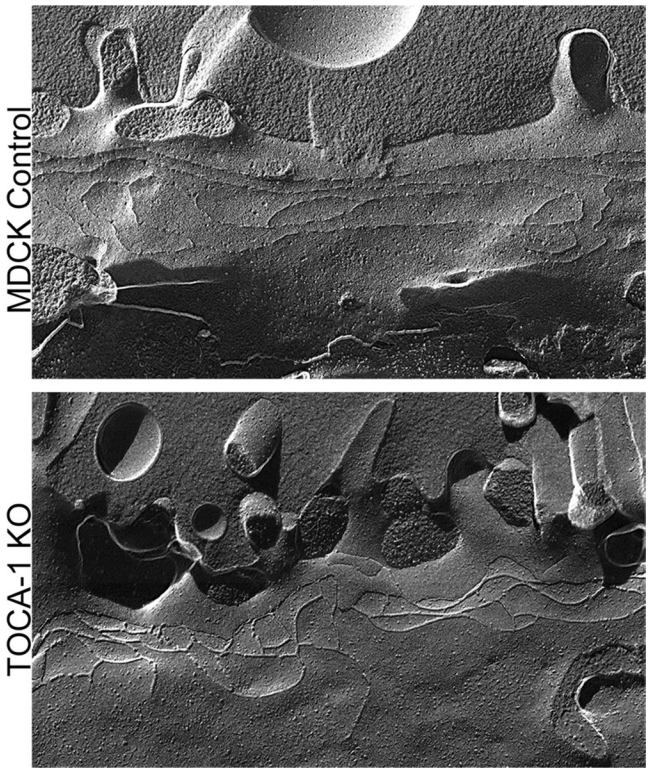

FIGURE 4: Freeze-fracture analysis of tight junctions from control and knockout MDCK cells does not reveal obvious differences in tight junction strand number or morphology. MDCK cells (top) and TOCA-1–knockout cells (bottom) were cultured on glass coverslips for 7 d, fixed with glutaraldehyde, and prepared for freeze fracture by a conventional protocol. Electron microscopic freeze-fracture analysis revealed similar-appearing tight junction strands.

we conclude that TOCA-1 is not required for the stable structure of junction strands, and the localization of tight and adherens junction proteins and its recruitment to the junction require a PDZ-dependent interaction with ZO-1. We next investigated a possible functional or dynamic role for TOCA-1 in maintaining the barrier.

Knockout of TOCA-1 results in increased paracellular permeability and delayed barrier recovery after calcium removal and replacement

Transepithelial electric resistance (TER), which measures the instantaneous electrical resistance of the paracellular barrier, was not different between MDCK controls and TOCA-1–knockout cells (Figure 5B, top graph). In contrast, paracellular flux as measured over 2 h with 3-kDa fluorescent dextran was consistently increased by greater than fivefold (Figure 5B) in knockdown cells over control cells. The findings of normal TER but increased flux are similar to those seen with ZO-1/ZO-2 double-knockdown cells (Fanning *et al.*, 2012) and have been interpreted to result from disruption of coupling with perijunctional actin and myosin. To test whether the increased flux in the knockdown cells was a function of the specific absence of the TOCA-1(+) isoform, we made stable cell lines in the TOCA-1–knockout background expressing either GFP TOCA-1(–) or GFP TOCA-1(+). Immunoblot analysis of MDCK control, knockout, and rescue cell lines probed with anti-TOCA-1 antibody (Figure 5A) demonstrated the completeness of knockout and the expression of the GFP-labeled rescue transgenes.

Expression of neither GFP-labeled rescue construct altered TER compared with control or knockout values, but expression of GFP TOCA-1(+) but not GFP TOCA-1(–) reversed the increase in flux seen in the knockout cells compared with controls. Localization of GFP-constructs in stably expressing cell lines (Figure 5C) confirmed the tight junction association of GFP TOCA-1(+) (Figure 5C, bottom row) but not GFP TOCA-1(–) (Figure 5C, third row). Together these data suggest although the absence of TOCA-1 does not affect the instantaneous barrier properties, tight junction-associated TOCA-1(+) is a functional component involved in maintenance of the longer–time frame dynamics of the paracellular "leak pathway" (Anderson and Van Itallie, 2009; Shen *et al.*, 2011).

Tight junction integrity is dependent on the presence of extracellular calcium; incubation of cells in low calcium (<50 μM) results in junction disassembly (Gonzalez-Mariscal *et al.*, 1985). After overnight culture in low-calcium media, both control MDCK and TOCA-1–knockout cells display equivalent loss of tight junction contacts, as detected by complete loss of TER (Figure 6A, time 0). Return of calcium resulted in recovery of TER in both control and knockout cell lines, but recovery was significantly delayed by ~1–2 h in knockout cells relative to controls (Figure 6A). This delay in tight junction assembly is paralleled by a delay in the recovery of continuous ZO-1 immunofluorescence along cell contacts (Figure 6B). At time 0, both control (Figure 6B, top) and TOCA-1–knockout cells (Figure 6B, bottom) have only small remnants of linear ZO-1 staining. By 1 h of calcium return, there is considerable linear ZO-1 staining in MDCK controls but not in TOCA-1–knockout cells. At 2 h of calcium return, TOCA-1–knockout cells begin to form linear ZO-1 contacts, but these are shorter and less continuous than in control cells. However, by 4 h after calcium return, both control and TOCA-1–knockout cells have normal-appearing ZO-1 staining. These findings are quantified by measurement of length of junctions as determined by ZO-1 staining in images of control and knockdown cells (Figure 6C). These data also show a 1- to 2-h delay in the recovery of tight junction staining.

TOCA-1–knockout cells show diminished long-term tight junction membrane dynamics compared with MDCK control cells

Because TOCA-1 had been implicated in endocytosis (Bu *et al.*, 2010) and tight junction protein endocytosis can regulate paracellular flux (Marchiando *et al.*, 2010), we used fluorescence recovery after photobleaching (FRAP) analysis to determine whether there were alterations in the short-term dynamics of ZO-1 or occludin that might be indicative of changes in the kinetics of tight junction endocytic recycling. MDCK control cells and TOCA-1–knockout cells were transiently transfected with GFP-ZO-1 or GFP-Ocln, and FRAP behavior was monitored in the midpoint of bicellular contacts. There was no difference in the mobile fraction or recovery kinetics of either protein between control and knockout cells (Supplemental Figure S3), suggesting that protein dynamics in the seconds range is not controlled by TOCA-1 to a measurable degree.

Although there are published data suggesting a role for TOCA-1 in endocytosis (Bu *et al.*, 2009), there is much stronger evidence that this protein plays a role in other aspects of plasma membrane dynamics, such as neurite elongation and filopodia formation (Kakimoto *et al.*, 2006; Bu *et al.*, 2009; Chander *et al.*, 2014). Given that epithelial cells in a monolayer shuffle and slide with respect to each other (Timpe *et al.*, 1978), we tested the possibility that TOCA-1 might play a role in tight junction membrane contact dynamics associated with normal cell movement. To do this, we transfected GFP ZO-1 into control and TOCA-1–knockout cells, imaged

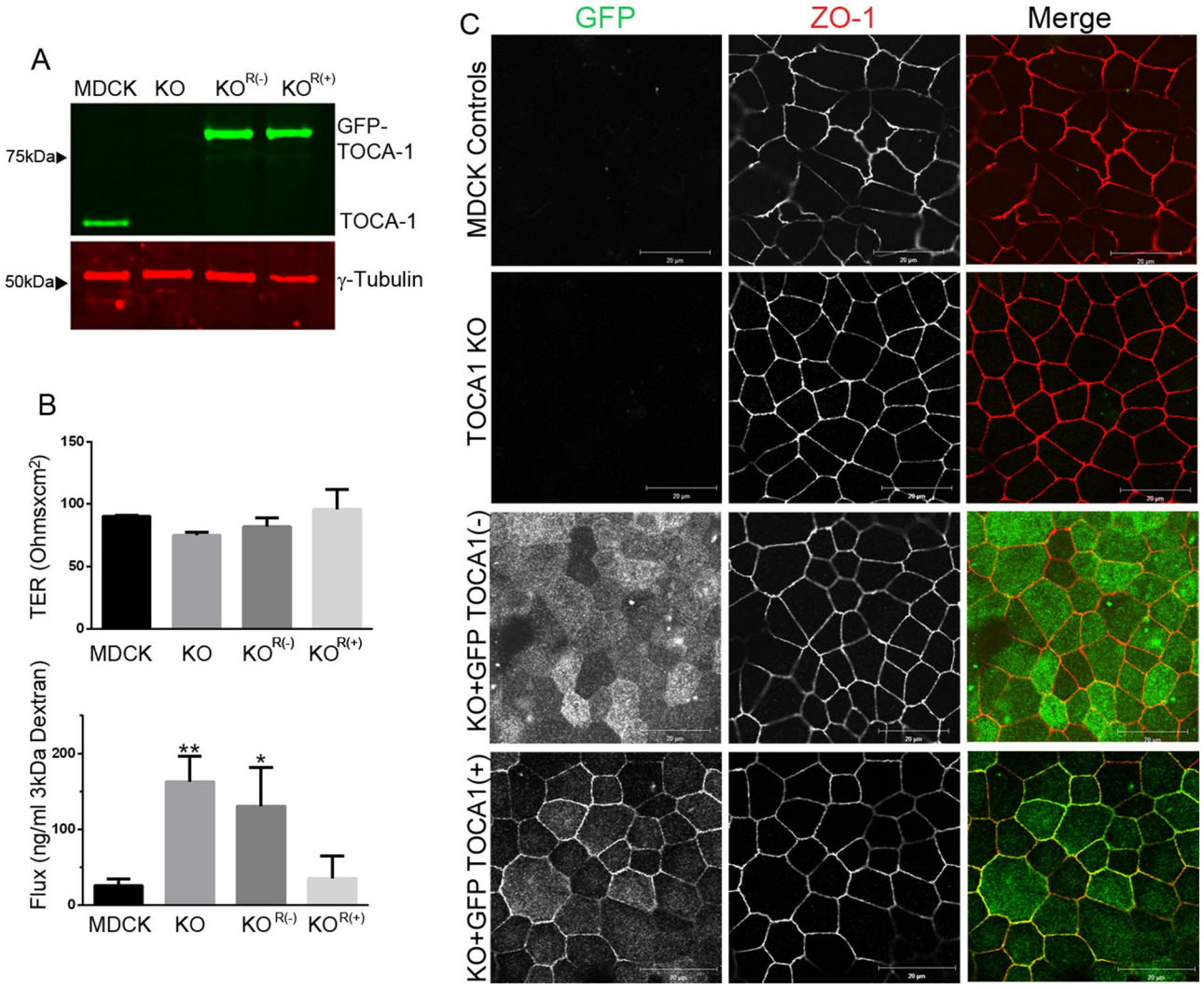

FIGURE 5: TOCA-1 knockout results in increased dextran flux that is rescued by expression of TOCA-1(+) but not TOCA-1(–) isoform. (A) Immunoblot of MDCK cells expressing endogenous TOCA-1 (left lane), knockout cells (middle lane), and knockout cell lines stabling expressing GFP TOCA-1(–) and GFP TOCA-1(+) (right lanes) probed with an anti-TOCA-1 antibody (top) or an anti–γ-tubulin antibody (bottom) shows slightly (~50%) higher levels of exogenous TOCA-1 expression. (B) TER of all cell lines was approximately equivalent (top; control, 91 ± 3; TOCA-1 knockout, 81 ± 5; GFP TOCA-1(–), 85 ± 5; GFP TOCA-1(+), 96 ± 7). Paracellular flux of 3-kDa fluorescent dextran (bottom) was fivefold higher in TOCA-1–knockout cells than with MDCK control cells. GFP TOCA-1(–) expression did not alter flux from that in knockout cells, whereas expression of GFP TOCA-1(+) returned dextran flux levels to values not significantly different from those in control cells (**$p < 0.001$, *$p < 0.01$ compared with control cells). (C) Immunofluorescence analysis of knockout MDCK cell lines showing diffuse localization of GFP TOCA-1(–) compared with junctional colocalization of GFP TOCA-1(+) with ZO-1. Bar, 10 μm.

the cells over 12 h, and viewed displacements of ZO-1 using full-depth confocal projections. The GFP ZO-1 signal in MDCK control cells (Supplemental Video1.mov) was consistently more spatially dynamic than in the TOCA-1–knockout cells (Supplemental Video2.mov). The most striking difference was the behavior of the micrometer-level movements—infoldings and outpouchings—of the cell–cell contacts as marked by GFP ZO-1. These were extremely active in control cells (Figure 7A, left). In contrast, the tight junction membrane in the knockout cells tended not only to be straighter (Supplemental Figure S4), but also showed very few of these small membrane wrinkles over this same time frame (Figure 7A, right). Time-lapse images of representative membrane regions show the dynamics of the inflections in the control but not the knockout cells (Figure 7B). The whole cell plasma membrane movement over the 12-h period was tracked using a membrane contact tracking program (QuimP11b; Tyson *et al.*, 2014); although this method did reveal differences between control and knockout cells, it underrepresented the degree of tight junction membrane movement in the control cells because in many cases the membrane inflections were too small to be detected by the resolution of the membrane segmentation program. Nevertheless, representative membrane tracks from control cells (Figure 7C, left) and TOCA-1–knockout cells (Figure 7C, right) clearly show that knockout cells have smoother membrane tracks than control cells. The changes in membrane contact dynamics were most obvious at the level of the tight junction, using GFP ZO-1 as a marker. Similar movies made with control and

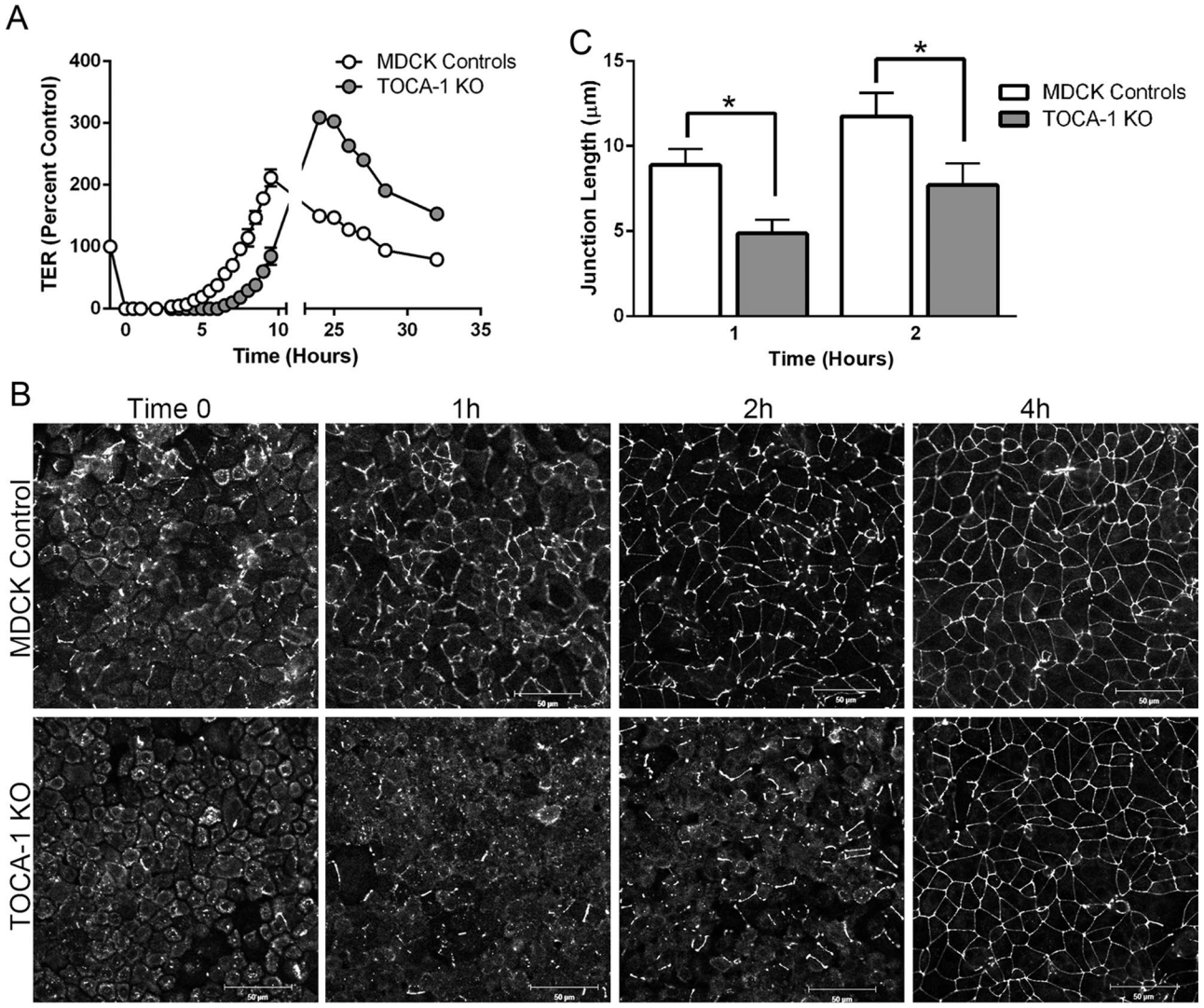

FIGURE 6: Knockout of TOCA-1 delays tight junction reassembly after calcium switch. (A) Confluent monolayers of filter-grown MDCK control and TOCA-1 knockout were incubated in low-calcium medium overnight (16 h) to disrupt junctions. TER was measured at the indicated periods after calcium readdition; whereas both control and knockout cells recovered barrier function, recovery was relatively delayed in knockout cells. (B) Immunofluorescence analysis of ZO-1 localization in control and knockout cells at selected times after calcium return demonstrates that linear ZO-1 staining is slower to recover in knockout cells than in control cells, although staining in both is relatively normal by 4 h. Bar, 50 μm. (C) The kinetics of recovery was confirmed by comparing the junction length as measured by ZO-1 staining using ImageJ; values were significantly different at both 2 and 1 h after calcium return (*$p < 0.0.1$). Representative of three separate experiments. Baseline TER was 128 ± 5 in control cells and 116 ± 7 in knockout cells.

knockout cells transfected with mEmerald E-cadherin did not show clear differences in membrane contact dynamics at the adherens junction or lateral membranes (control, Supplemental Video S1. mov, and TOCA-1 knockout, Supplemental Video S2.mov). These results suggest that TOCA-1 influences dynamics specifically at the tight junction seal.

To verify that changes in membrane contact dynamics were associated with the loss of TOCA-1(+) isoform, we cotransfected TOCA-1–knockout cells with GFP ZO-1 and either mRed TOCA-1(–) or mApple TOCA-1(+). We also expressed mApple TOCA-1(+) with a mutation in the SH3-binding domain known to inhibit binding to N-WASP (W518K) to test the idea that TOCA-1 might affect contact movement through N-WASP–dependent actin dynamics. The coexpression of both GFP and mRed or mApple in individual cells was verified at the beginning of the 12-h imaging period (Figure 7D); mRed TOCA-1(–) did not colocalize with ZO-1 (Figure 7D, top row), but, as expected, a fraction of both the mApple TOCA-1(+) (Figure 7D, middle row) and mApple TOCA-1(+)W518K (Figure 7D, bottom row) did colocalize with GFP ZO-1. Because the GFP signal was far more stable than that of any of the red fluorescent proteins tested, it alone was imaged over 12 h. Movies and membrane contact tracking, as described, for a representative cell expressing both GFP ZO-1 and mRed TOCA-1(–) demonstrated that it did not appear different from knockout cells without TOCA-1 (Supplemental Video 3.mov and Figure 7D, top). In contrast, expression of mApple TOCA-1(+) restored the dynamic tight junction phenotype seen in control MDCK cells (Supplemental Video 4.mov and Figure 7D, middle). In contrast, the behavior of GFP ZO-1 in cells expressing

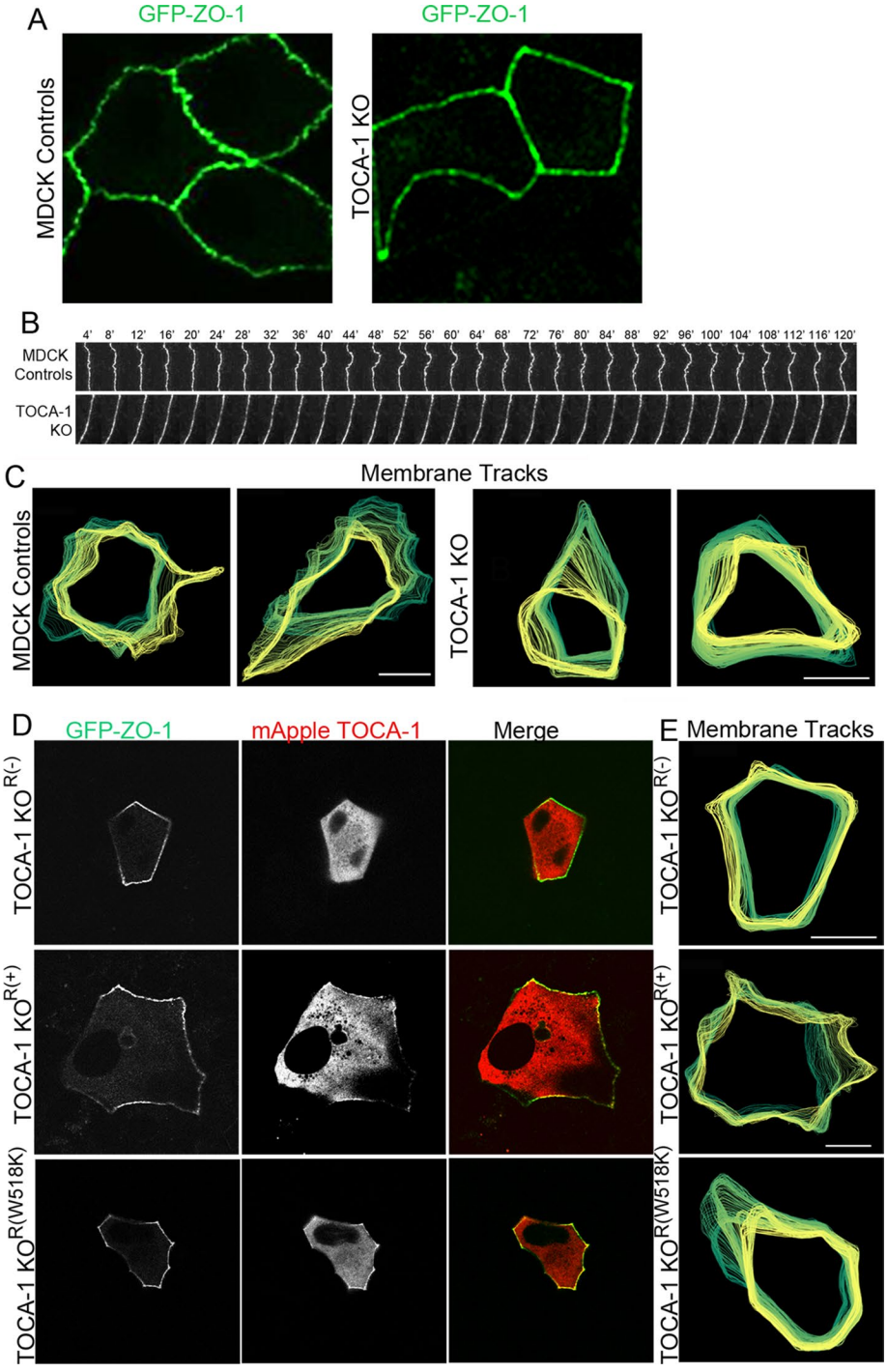

FIGURE 7: TOCA-1–knockout cells showed decreased tight junction membrane contact dynamics compared with MDCK controls. (A) MDCK control (left) and TOCA-1–knockout (right) cells transiently expressing GFP ZO-1 were imaged overnight. (B) Time-lapse images from representative regions are shown at 4-min intervals during a 2-h window within the 12-h imaging period. (C) GFP ZO-1 membrane traces of two representative controls (left) and TOCA-1–knockout cells (right); images were taken every 4 min for 12 h; image color grades from blue to yellow with time. Bar, 5 μm. (D) TOCA-1–knockout cells were transfected with GFP ZO-1 and mRed-TOCA-1(–) (top), mApple TOCA-1(+) (middle), or mApple TOCA-1(+) W518K (bottom). Images were taken at the start of 12-h imaging period as before to verify coexpression of fluorescently labeled ZO-1 and TOCA-1. (E) Representative GFP ZO-1 membrane tracks from TOCA-1–knockout cells expressing TOCA-1(–) (top), TOCA-1(+) (middle), and TOCA(+)W518K (bottom) as shown in left-hand images. Bar, 5 μm.

mApple TOCA-1(+)W518K was not different from that of the knockout cells alone (Supplemental Video 5.mov and Figure 7D, bottom), suggesting that the dynamics requires a functional SH3 domain.

TOCA-1(+) recruits N-WASP and WIPF2 to tight junctions

A critical mediator in the ability of TOCA-1 to influence actin polymerization is known to be through its interaction with N-WASP (Ho *et al.*, 2004). Immunoblot analysis (Figure 8A) of control MDCK cells and TOCA-1–knockout cells revealed no differences in the global levels of N-WASP, the N-WASP–binding protein WIPF2, or the WASP family member WAVE2. In spite of employing a variety of different methods, we found it difficult to image endogenous N-WASP at MDCK cell junctions, but expression of GFP TOCA-1(+) in knockout cells resulted in the easily detectable recruitment of N-WASP (Figure 8B, top row) and WIPF2 (Figure 8B, third row) to colocalize with ZO-1 at cell contacts. In contrast, GFP TOCA-1(+)W518K failed to recruit either N-WASP or WIPF2 (Figure 8B, second and fourth rows, respectively). The distribution of WAVE2, which was more easily detected than endogenous N-WASP or WIPF2, appeared to be concentrated slightly basal to ZO-1, and its distribution was not altered by expression of GFP TOCA-1(+) (Figure 8B, bottom row). We were unable to detect significant junction localization of the Arp2/3 complex member Arp3 or Cdc42 in control or knockout cells.

Knockout of TOCA-1 results in the accumulation of actin at the adherens junction

WASP family members are involved in the regulation of Arp2/3-dependent branched actin nucleation (Rohatgi *et al.*, 1999). We therefore examined the distribution of F-actin as reported by rhodamine–phalloidin staining in MDCK control and knockdown cells. En face confocal imaging of filter-grown control (Figure 9A, top) and knockout cells (Figure 9A, bottom) suggested that F-actin was relatively more concentrated at the apical junctional complex in knockdown cells and had a slightly different distribution than in control cells; it was spread in a wider ring along the plasma membranes. In *Z*-section images of control cells (Figure 9B, top), F-actin was distributed fairly evenly along the lateral cell membrane from the base of cells to the apical domain, with a slight concentration at the apical end of the lateral

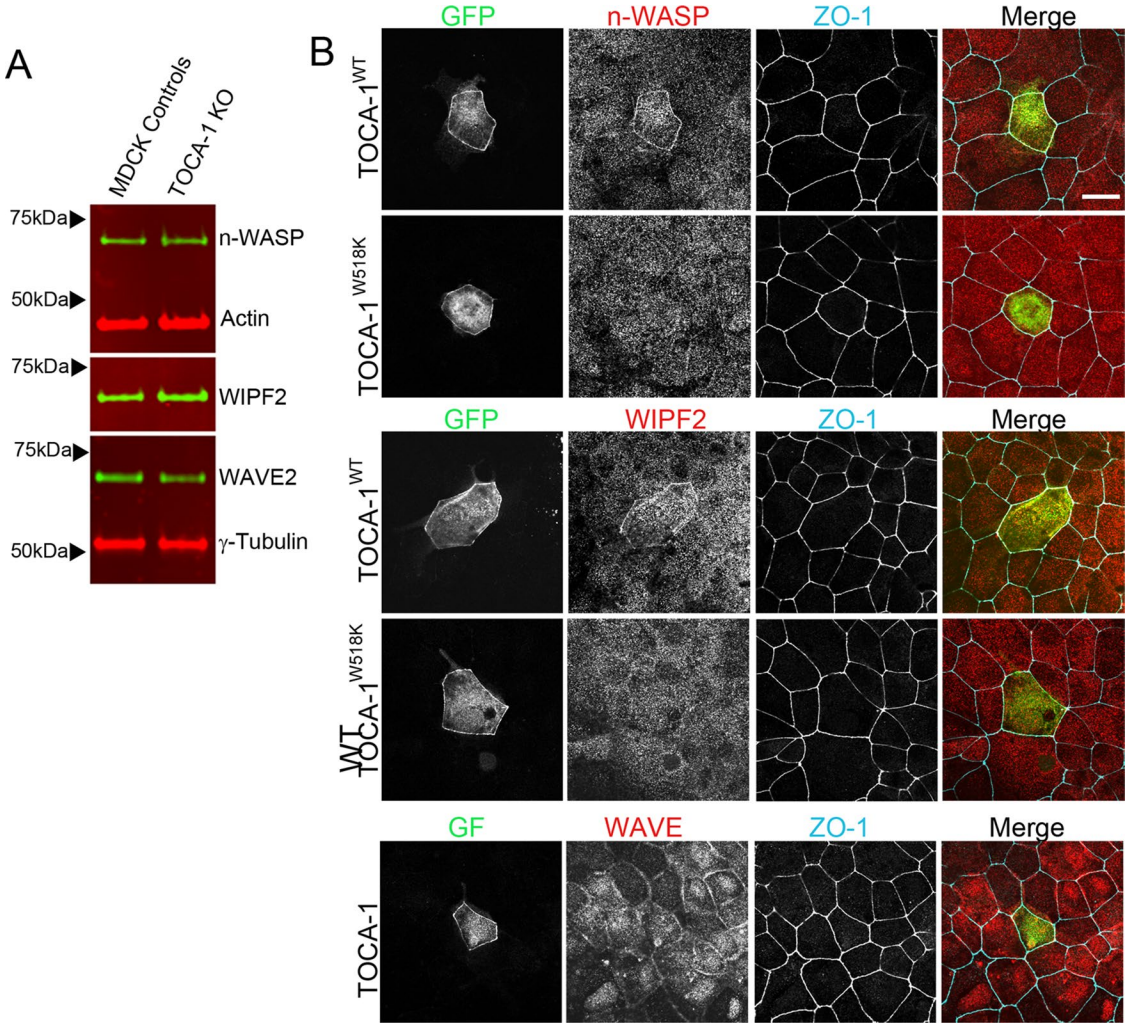

FIGURE 8: GFP TOCA-1 recruits nWASP and WIPF2 but not WAVE to tight junctions in TOCA-1–knockout cells. (A) Immunoblot analysis of WASP family members in control and TOCA-1–knockout cells reveals no differences in the expression levels of N-WASP, WIPF2, and WAVE2. (B) Immunofluorescence analysis of transient expression of GFP TOCA-1(+) in TOCA-1–knockout cells results in recruitment of N-WASP (top row) and WIPF2 (third row) but not WAVE2 (bottom row). In contrast, expression of GFP TOCA-1(+) with a mutation in the SH3-binding domain (W518K) no longer recruits N-WASP (second row) or WIPF2 (fourth row). Bar, 10 μm.

membrane. In contrast, lateral actin in TOCA-1–knockout cells appeared like a lollipop, with very bright actin staining in the apicolateral cell membrane relative to the rest of the lateral membrane.

This difference in actin distribution was confirmed in TEM images of control and knockout cells. In MDCK control cells, there is normally little actin condensation evident at the tight or adherens junctions (Figure 9C, left; Fanning *et al.*, 2012). In contrast, there is obvious actin accumulation at the adherens junction in TOCA-1–knockout cells (Figure 9C, middle two images), and this is recapitulated in control cells treated with the Arp2/3 inhibitor CK666 (Figure 9C, right).

We were unable to reliably detect differences between control and knockout cells in actin polymerization rates at the cell contacts using fluorescent G-actin accumulation assays. This may be due to our inability to discriminate at the light microscopic level between tight and large adherens junction actin pools and the multiplicity of reported pathways for actin polymerization at the adherens junction. However, treatment of control MDCK cells with the Arp2/3 inhibitor CK666 (Hetrick *et al.*, 2013) resulted in a similar increase in flux seen in the TOCA-1–knockout cells (Figure 9D), consistent with a requirement for continuous branched actin nucleation in maintaining the paracellular barrier. Further, CK666 administration to TOCA-1–knockout cells resulted in a synergistic increase in flux (Figure 9D). Arp2/3 activity is regulated by multiple pathways (Rotty *et al.*, 2013), but the increased sensitivity of knockout cells to CK666 suggests that endogenous Arp2/3 activity may be decreased in these cells such that further inhibition of this actin nucleation pathway has much more dramatic effects than is seen in control cells after treatment with the inhibitor. Live-cell imaging of MDCK control cells transfected with GFP ZO-1 with and without treatment with CK666 results in a similar decrease in tight junction membrane dynamics seen in the TOCA-1–knockout cells (vehicle-treated cells, Supplemental Video 6.mov, and CK666-treated cells, Supplemental Video 7.mov); this was also seen in the membrane tracks on comparing vehicle-treated (Figure 9E, top) to CK666-treated (Figure 9E, bottom) MDCK cells.

To test whether the decreased membrane dynamics seen in the TOCA-1–knockout cells was due to altered junctional tension, we cut cell junctions in GFP ZO-1–expressing control and knockout cells

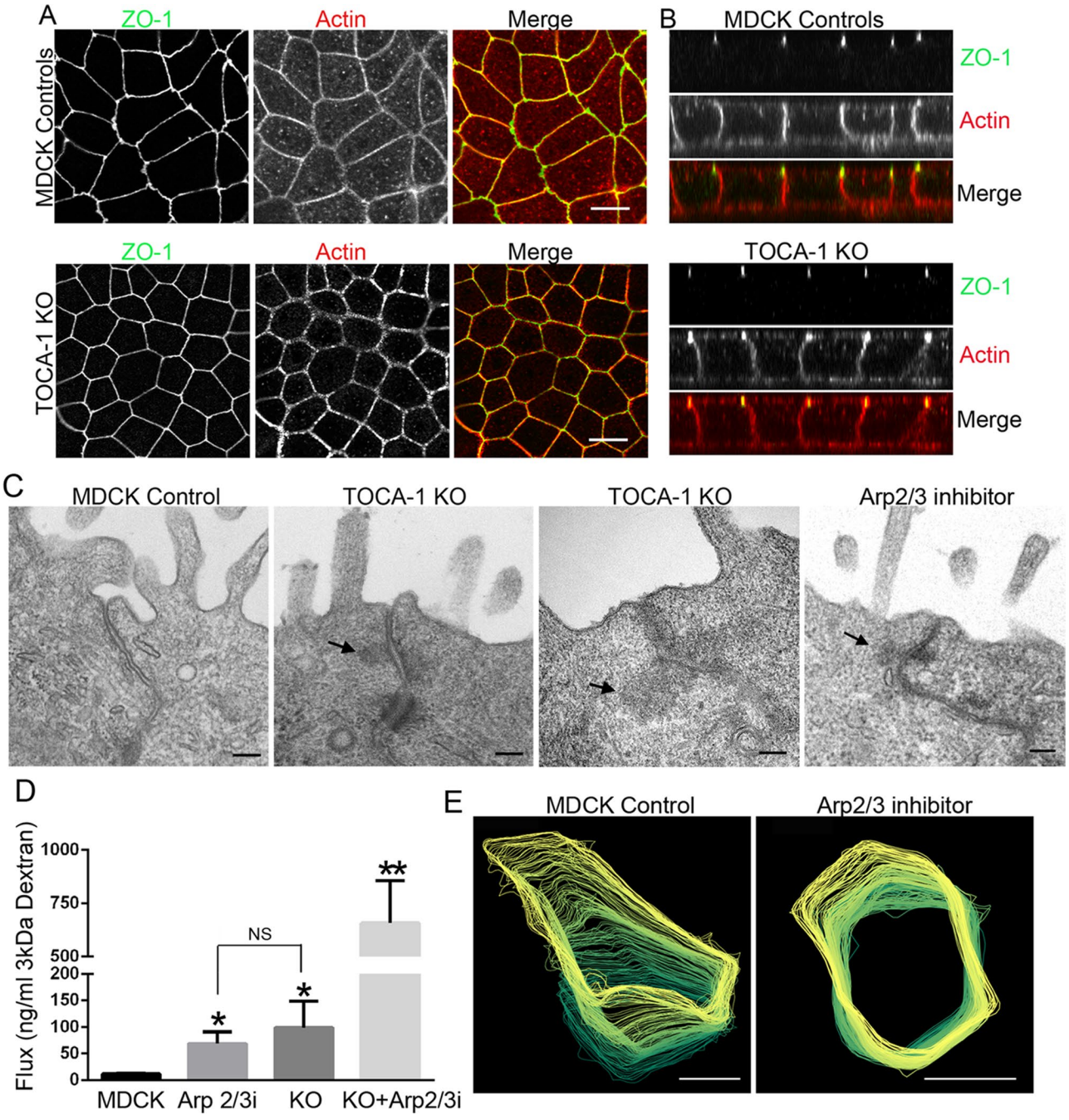

FIGURE 9: TOCA-1 knockout results in actin accumulation at the adherens junction. (A) En face confocal immunofluorescence analysis of F-actin apical junctional actin localization in MDCK control (top) and TOCA-1–knockout cells. Bar, 10 μm. (B) Z-stack images of MDCK control (top panels) and TOCA-1 knockout cells (bottom) stained with ZO-1 and rhodamine–phalloidin for F-actin localization shows actin accumulation at the apical junction in TOCA-1–knockout cells. Lateral actin levels appear approximately equivalent in the two cell lines. (C) TEM images from the apical junctional region of MDCK control cells (left) and TOCA-1 knockout cells (middle two) reveals relative accumulation of actin at the adherens junction in the knockout cell lines (arrows). Accumulation of apical junctional actin is also evident in MDCK control cells treated for 2 h with 100 μM of the Arp2/3 inhibitor CK666 (right). Bar, 100 nm. (D) Flux of fluorescent 3-kDa dextran is increased in MDCK controls treated with the Arp2/3 inhibitor CK666 (100 μM); this increase is markedly greater in CK666-treated TOCA-1– knockout cells (*$p < 0.01$, **$p < 0.001$). (E) Representative membrane tracks from live-cell imaging of GFP ZO-1–transfected MDCK control and Arp2/3-treated cells. Bar, 5 μm.

with laser nanoscissors and monitored the degree of separation of the adjacent cell vertices (Figure 10). Yap and coworkers (Verma *et al.*, 2012) previously demonstrated that cutting the adherens junction membrane in Caco-2 cells, as detected with GFP–E-cadherin, resulted in a large and rapid separation of the adjacent cell vertices. In contrast to Caco-2 cells, the separation was detectable but less in MDCK control cells cut with laser nanoscissors as detected with GFP ZO-1 (Figure 10, A, top, and B, open circles). This could be due to

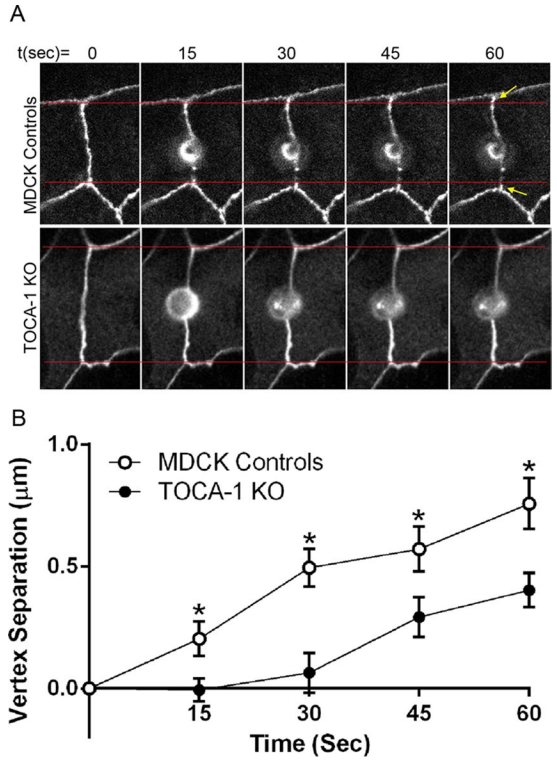

FIGURE 10: TOCA-1 knockout results in decreased tension along the tight junction. (A) Image sequence of tight junctions labeled by GFP ZO1 after laser scission reveals that the tight junction in control cells (top) is under a small degree of tension, as indicated by separation of the adjacent cell vertices; the red lines indicate the starting positions of the vertices, and vertex separation is evident at 60 s (top, yellow arrows); quantified in B (open circles, $n = 34$). In contrast, laser scission of junctions in TOCA-1– knockout cells shows little separation of cell vertices: image sequence in A, bottom; quantified in B (closed circles, $n = 24$; $*p < 0.05$).

cell-type differences or reflect a difference in tension at the adherens and tight junctions as detected by behavior of the different localizations of the GFP-tagged protein markers. The latter would be consistent with the idea that adherens and not tight junctions are the major sites for apical contractility (Sawyer *et al.*, 2010). In TOCA-1–knockout cells, there was even less robust separation than that seen in controls after membrane scission (Figure 10, A, bottom, and B, closed circles), suggesting that the straight membranes and lack of membrane dynamics seen in knockout cells are not due to increased junctional tension within the monolayer. The finding of decreased vertex separation seen in the knockout cells is instead consistent with decreased activity of Arp2/3, since Arp3 knockdown in Caco-2 cells also results in diminished membrane expansion (Verma *et al.*, 2012).

TOCA family member formin-binding protein 1 but not Cdc42-interaction protein 4 has a similar isoform with a putative PDZ- binding motif

TOCA-1 is a member of a subfamily of closely related F-BAR domain–containing proteins (Ho *et al.*, 2004) that includes formin-binding protein 17 (FBP17; Kamioka *et al.*, 2004) and Cdc42-interacting protein 4 (CIP4; Aspenstrom, 1997). FBP17 but not CIP4 was identified as proximal to ZO-1 in our original BioID screen (Van Itallie *et al.*, 2013). Inspection of sequence databases revealed that FBP17 contained a similar splice form with a carboxyl-terminal putative PDZ- binding motif as is found in TOCA-1 (Figure 11A). In contrast, the third member of the TOCA family, CIP4, lacks a putative PDZ-binding motif. Immunofluorescence localization of endogenous FBP17 in MDCK cells showed that this protein weakly colocalized with ZO-1 in MDCK cells, although much of the FBP17 was distributed throughout the cytoplasm (Figure 11B, top row); transiently transfected GFP FBP17(+) but not GFP FBP17(-) partially colocalized with ZO-1 (Supplemental Figure S5). In contrast, CIP4 did not concentrate with ZO-1 at tight junctions but was instead distributed throughout the cells (Figure 11B, bottom row). CIP4 has been implicated in controlling cadherin endocytosis (Leibfried *et al.*, 2008; Rolland *et al.*, 2014; Zobel *et al.*, 2015). Together these results lead to speculation that FBP17, but not CIP4, might serve a function similar to TOCA-1 at the tight junction.

qRT-PCR showed that transcripts for FBP17 isoforms containing (FBP17(+)) and lacking (FBP17(–)) the putative PDZ-binding motif sequences were expressed in MDCK cells (Figure 11C, top graph), with slightly more of the FBP17(+) than FBP17(–) isoform expressed; FBP17(+) transcript was expressed at ~60% of the level of TOCA-1(+) relative to ZO-1 transcript expression in MDCK cells. In contrast, in human primary dermal fibroblasts and HEK 293 cells, more FBP17(–) transcript was expressed relative to FBP17(+) (Figure 11C, bottom two graphs). In these two cell lines, the predominant TOCA-1/FBP17 transcript form was FBP17(–). To determine whether FBP17 knockout in MDCK cells would potentiate the effects seen with TOCA-1 knockout, we made CRISPR-mediated double-knockout cell lines. After selection, dilution cloning, and screening by immunoblotting, we used PCR to amplify genomic DNA around the putative mutation site. Sequencing of the PCR product revealed a 2–base pair deletion that resulted in a frameshift and stop codon after amino acid residue 75 (Figure 11D). Analysis of double-knockout clones by immunoblot confirmed the loss of TOCA-1 and FBP17, with no effect on the levels of the third TOCA family member, CIP4 (Figure 11E).

Paracellular flux in control, TOCA-1–knockout, and TOCA-1/FBP17 double-knockout cells showed no significant difference between the single- and double-knockout cells (Figure 11F). In addition, live-cell imaging of GFP ZO-1–transfected double-knockout cells revealed a decrease in tight junction membrane dynamics that was indistinguishable from the single–TOCA-1–knockout cells (control cells, Supplemental Video S3.mov, and TOCA-1/FBP17 double-knockout cells, Supplemental Video S4.mov and Figure 11G). Finally, TEM analysis of TOCA-1/FBP17 double-knockout cells showed increased adherens junction actin accumulation (Figure 11H, right, arrow) similar to that seen in the single–TOCA-1–knockout cells. Together these results do not support an additive or synergistic role for FBP17 in tight junction barrier dynamics.

DISCUSSION

Much evidence exists for the importance of actin and actin-regulating proteins in controlling the tight junction barrier (Rodgers and Fanning, 2011; Zhou *et al.*, 2013), but there is less understanding of how tight junction proteins are functionally and dynamically coupled to actin organization. In the present study we provide the unexpected observation, based initially on BioID proteomics, that an alternatively sliced PDZ-binding motif on TOCA-1 binds it to ZO-1, bringing N-WASP and its actin-regulatory activity directly to the tight junction. Knockout of TOCA-1 results in increased paracellular flux and suppression of junction membrane contact dynamics, which we speculate is required to maintain the cell-to-cell seal. There is ample evidence that endocytosis (Marchiando *et al.*, 2010) and

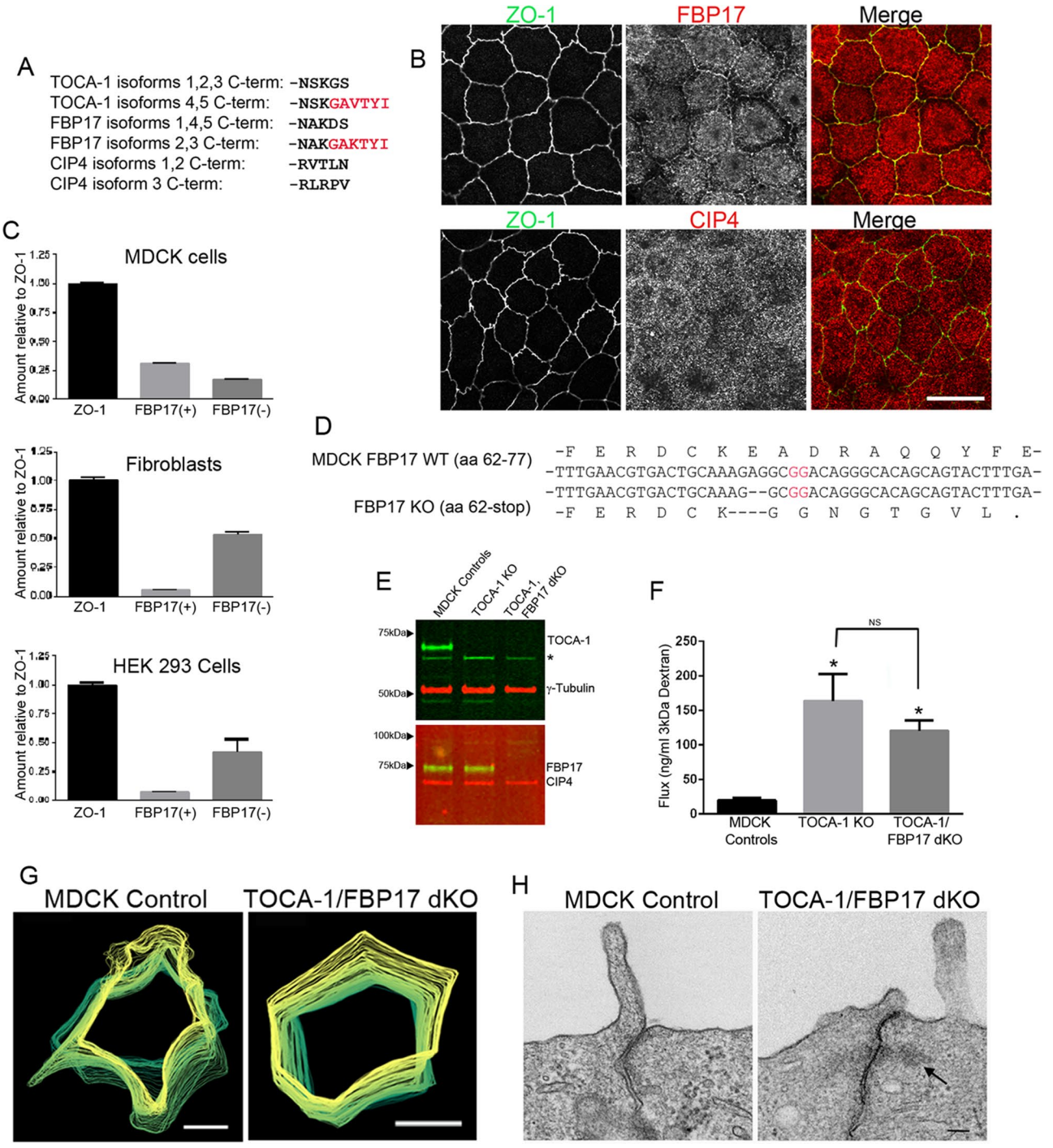

FIGURE 11: Double knockout of TOCA-1 and the TOCA-1 relative FBP17 does not further impair barrier function or adherens junction actin accumulation. (A) Comparison of isoform sequences of members of the TOCA-1 subfamily of F-bar proteins shows that FBP17 but not CIP4 has splice forms that contain putative PDZ-binding motifs (in red). (B) Immunofluorescence analysis of MDCK cells stained for ZO-1 (right) and FBP17 (top middle) reveals weak colocalization (merge, top right). In contrast, CIP4 (middle bottom) fails to colocalize with ZO-1 (merge, bottom right). Bar, 10 μm. (C) qRT-PCR shows greater expression of FBP(+) than FBP(–) isoforms (approximately twofold) in MDCK cells, whereas two nonepithelial cell lines (primary human dermal fibroblasts and HEK 293 cells) had fivefold higher expression of FBP(–) mRNA than FBP(+) mRNA. (D) Sequencing of PCR products amplified from genomic MDCK cell showed knockout cells had a 2–base pair deletion upstream of the PAM site (red GG), resulting in a frameshift in the FBP17 coding sequence with a premature stop codon at amino acid 75. (E) Immunoblot analysis confirms the loss of TOCA-1 and FBP17 in double-knockout cells, with no change in CIP4 levels. Asterisk indicates nonspecific band. (F) Comparison of dextran flux in control, TOCA-1 single-knockout cells, and TOCA-1/FBP17 reveals no significant different in flux between single- and double-knockout cell lines. (G) Membrane tracings from live-cell imaging from GFP ZO-1–transfected control and double-knockout cells reveals a similar decrease in tight junction membrane dynamics as seen in TOCA-1–knockout cells. Bar, 5 μm. (H) TEM reveals similar accumulation in adherens junction actin (arrow) in double-knockout cells as seen in TOCA-1–knockout cells. Bar, 100 nm.

myosin ATPase activity (Cunningham and Turner, 2012) are important regulators of the barrier. Our results support a further requirement for branched actin growth under the junction facilitating dynamic cell-to-cell contact remodeling to maintain the paracellular barrier.

TOCA-1 interaction with ZO-1 was verified using both immunolocalization of GFP TOCA-1(+) and biochemical assays. Recognition of this PDZ-targeting mechanism suggests a previously unappreciated, spatially focused role for TOCA-1; most published results in mammalian systems have depended on exogenous expression of a TOCA-1 isoform lacking the PDZ-binding motif (Kakimoto *et al.*, 2006; Bu *et al.*, 2009, 2010). Junction localization of TOCA-1 has been described in *C. elegans,* which has two isoforms, one of which is enriched at cell junctions (Giuliani *et al.*, 2009) and required to organize junctional actin and the junction-associated protein AJM-1. However, it lacks a PDZ-binding motif, and the mechanism of its localization to cell contacts is not clear. The expression of both (+) and (–) isoforms was confirmed by qRT-PCR, which also demonstrated that in epithelial cells, the relative expression levels of the (+) isoform were higher than those of the (–) isoform. In contrast, transcript levels for both (+) and (–) isoforms were lower but equivalent in nonepithelial cells. These results are consistent with a specific epithelial role for the TOCA-1(+) isoforms, presumably requiring its localization to tight junctions by binding ZO-1.

Of the three members of the TOCA family in mammals (Ho *et al.*, 2004; TOCA-1, FBP17, and CIP4), FBP17, like TOCA-1, has similar splice forms containing and lacking PDZ- binding motifs; it too was identified in the ZO-1 proteomics screen, although it was recovered at a considerably lower level (Van Itallie *et al.*, 2013). Like TOCA-1, transcript levels for FBP17(+) are relatively enriched in MDCK cells, whereas in contrast, FBP17(–) transcripts predominate in the two nonepithelial cells tested. The colocalization of FBP17(+) with ZO-1 is less robust than that of TOCA-1, and knockout of FBP17 on top of the TOCA-1 knockout did not further enhance the flux and movement defects. Despite our inability to make an FBP17 single knockout, the evidence does not suggest that FBP17 is separately critical for the functions we characterized. The third mammalian TOCA family member, CIP4, was not identified in any of the tight junction proteomic screens (Van Itallie *et al.*, 2013; Fredriksson *et al.*, 2015) and lacks a similar PDZ-binding motif–containing splice form; in contrast, it has well-characterized roles at the adherens junction (Rolland *et al.*, 2014; Zobel *et al.*, 2015). Thus addition of the PDZ-binding motif appears to be a mechanism for targeting two of these three highly homologous WASP-binding BAR-domain proteins specifically to the tight junction.

Comparison of TOCA-1–knockout cells with controls did not reveal any obvious differences in the static organization of tight junction proteins or their levels. In addition, TER between control and knockout cells was similar. However, finding that TOCA-1 knockout resulted in the increased paracellular flux underscores much previous data (Balda *et al.*, 1996; Shen *et al.*, 2011) demonstrating different mechanisms regulating instantaneous barrier function, as measured by TER, and those regulating longer-term barrier dynamics as measured by flux. TER is largely influenced by the claudin protein profile (Van Itallie and Anderson, 2006), whereas changes in actin organization and actomyosin contractility have been implicated in controlling paracellular flux (Zolotarevsky *et al.*, 2002; Clayburgh *et al.*, 2005). In addition, increased flux has in some cases shown to be dependent on occludin endocytosis (Marchiando *et al.*, 2010), and recent studies have linked this to alterations in occludin dynamics detectable by FRAP analysis (Buschmann *et al.*, 2013). However, we saw no difference in the FRAP behavior of GFP occludin or GFP ZO-1 in our TOCA-1 knockouts compared with MDCK control cells, suggesting that TOCA-1 does not regulate short-term dynamics of tight junction protein interactions but more likely works by controlling actin dynamics.

Unexpectedly, examination of tight junction dynamics over a much longer scale uncovered a dramatic difference between MDCK control cells and TOCA-1–knockout cells. Using GFP ZO-1 as a probe, we found that over 12 h, the tight junction membrane contacts undergo continual small shape changes, forming constant small convex and concave inflections. The constant mobility of these small shape changes is lost in the TOCA-1–knockout cells; in these cells, the membrane at the level of the tight junction tends to maintain very smooth borders over the same time period. These constant tight junction membrane movements may depend on the ability of TOCA-1 to recruit and activate N-WASP and thus stimulate Arp2/3-dependent branched actin nucleation.

Although N-WASP has been reported to localize to tight junctions (Ivanov *et al.*, 2005), by immunofluorescence we see little endogenous N-WASP at either tight or adherens junction in MDCK cells. However, both N-WASP and its binding protein WIPF2 were identified as ZO-1–proximal proteins in our earlier BioID screen (Van Itallie *et al.*, 1995), and exogenous TOCA-1(+) expression is capable of recruiting them to tight junctions. We thus speculate that the TOCA-1(+)/N-WASP/WIPF2 complex is physiologically relevant at tight junctions but present at low levels; this is supported by the finding that decreased membrane dynamics in knockout cells can be rescued by expression of GFP TOCA-1(+) but not by a construct with a mutation in its SH3 domain that blocks binding to N-WASP. However, it is possible that tight junction–associated N-WASP may have other roles beyond induction of actin polymerization. A recent article by Yap and coworkers (Kovacs *et al.*, 2011) found that N-WASP was important in actin stabilization rather than nucleation. Instead of or along with N-WASP, TOCA-1 could be interacting with another SH3-binding protein, for example, the N-WASP family member WAVE2 (Fricke *et al.*, 2009; Giuliani *et al.*, 2009). However, although WAVE2 is readily detectable in MDCK cells, unlike N-WASP and WIPF2, it was not recovered in the ZO-1 BioID assays (Van Itallie *et al.*, 2013) nor did it accumulate with GFP TOCA-1(+) at apical cell contacts. Others have demonstrated a role for WAVE2 in actin organization at adherens junctions (Verma *et al.*, 2012; Han *et al.*, 2014), and we find that its distribution in MDCK cells would be more consistent with a role at adherens junction than at the tight junction. The contribution of WIPF2 to the observed tight junction membrane dynamics is unclear, but the related protein WIP has been reported to suppress N-WASP activity in the absence but not the presence of TOCA-1 (Martinez-Quiles *et al.*, 2001; Ho *et al.*, 2004; Takano *et al.*, 2008), and WIPF2 itself has been reported to mediate effects of N-WASP at the adherens junction (Kovacs *et al.*, 2011).

Although we were unable to show directly that knockout of TOCA-1 caused specific changes in tight junction actin incorporation rates, the use of the Arp2/3 inhibitor CK666 supported a role for this protein complex, since CK666 administration to MDCK control cells resulted in both increased flux and in decreased tight junction membrane dynamics similar to that seen in the TOCA-1–knockout cells. Arp2/3-mediated membrane dynamics were previously implicated in VE-cadherin–based junctions of endothelial cells (Abu Taha *et al.*, 2014). Activation of Arp2/3 would be expected to stimulate branched actin assembly (Rotty *et al.*, 2013); this activity, when focused at the tight junction through TOCA-1(+)/N-WASP activation, could explain the observed local membrane deformations. Branched actin assembly is associated with the formation of

lamellipodia (Chhabra and Higgs, 2007), and thus the increased membrane dynamics could be primarily due to Arp2/3 branched actin assembly pushing on the membrane, similar to lamellipodia formation, but constrained to the tight junction. Alternatively, branched actin assembly is also associated with endocytosis (Mooren *et al.*, 2012), so although we see no obvious difference in ZO-1 endocytosis in control and knockout cells in our time-lapse studies or in the FRAP behavior, we cannot rule out a role for altered endocytosis contributing to the observed changes. This will be a focus for further studies.

The mechanism for increased flux could be directly or indirectly a function of the differing membrane dynamics. We hypothesize that these small membrane fluctuations could constantly and flexibly adjust the tension on tight junction seals as the cells move against each other in a monolayer or in response to cell division or apoptosis. One possibility then is that the more static membranes of the TOCA-1–knockout cells may be less adaptable to changes in monolayer tension, resulting in temporary breaks in the tight junction barrier and increased paracellular flux. An alternative explanation is that these are two separable processes and that the flux increase is due to apical junctional actomyosin contraction, a mechanism that has been described previously (Cunningham and Turner, 2012; Fanning *et al.*, 2012). This is also consistent with the accumulation of adherens junction actin we observe by electron microscopy. However, the decreased degree of vertex separation in the knockout cells relative to control cells after laser scission and the findings that both myosin 2B levels and localization and phospho-myosin staining were similar in control and knockout cells (Supplemental Figure S6) are not consistent with increased tension on the junctions within the monolayer. It is possible that differing membrane motility and increased adherens junction actin could both be responses to decreased Arp2/3-dependent actin nucleation at the tight junction. Several studies have suggested that TOCA family members can participate in reciprocal inhibition of branched and linear actin formation (Yan *et al.*, 2013). Thus removal of tight junction TOCA-1 may disinhibit other local actin polymerization pathways, such as formin-dependent pathways, leading to increased linear actin at the adherens junction. However, this is highly speculative, and it is clear that there are multiple pathways of actin assembly at the adherens junctions such that it is difficult to implicate a single one in the increased actin seen in the TOCA-1 knockouts.

Many of the results observed in the TOCA-1–knockout cells recapitulate findings in the ZO-1/ZO-2 double-knockdown cells (Fanning *et al.*, 2012), which also lack TOCA-1(+) at cell contacts; this includes normal TER and increased flux. Strikingly, ultrastructural analysis demonstrates that the TOCA-1 knockout, like the ZO1/2 double knockdown, also results in actin accumulation at the adherens junction (Fanning *et al.*, 2012). Together these results suggest the possibility that TOCA-1 may be downstream of ZO-1 in this aspect of tight junction regulation. However, the ZO-1/2 double knockdown shows increased apical constriction and more obvious Myo2B and phospho-myosin staining than is seen in the TOCA-1–knockout cells, suggesting that ZO proteins play roles in additional pathways.

In this study, we demonstrate that TOCA-1(+) is recruited to tight junctions and can influence actin organization, likely through recruitment of N-WASP. However, TOCA-1 is a multidomain protein, and other domains, specifically the F-BAR domain, may also act to regulate the tight junction. Although TOCA-1(+) is recruited to tight junctions by its interaction with ZO-1, it presumably can bind membranes and may influence membrane shape. In addition to bending membranes, BAR domains can sense curvature (Shimada *et al.*, 2007); we are thus interested in exploring whether TOCA-1 senses curvature produced by tension at barrier contacts and whether this activity is important in the promotion of actin assembly (Takano *et al.*, 2008). Alternatively, TOCA-1(+) may influence membrane lipid composition; a recent study demonstrated that F-Bar domains can create distinct lipid microdomains in artificial membranes and cells (Zhao *et al.*, 2013). This may contribute to formation of the distinct lipid microdomains known to exist at the tight junction (Nusrat *et al.*, 2000). Finally, the identification of several other BAR domain–containing proteins as proximal to tight junctions, including BIN3 (Van Itallie *et al.*, 2013), pacsin2, and IRSp53 (Fredriksson *et al.*, 2015), suggests that there may be common themes in barrier regulation to be uncovered.

MATERIALS AND METHODS

Cell culture and transfections

MDCK II and Caco-2 cells were obtained from the American Type Culture Collection (ATCC, Manassas, VA) and maintained at 37°C, 5% CO_2. MDCK II cells were maintained in high-glucose DMEM (Mediatech, Manassas, VA; 4.5 g/l), supplemented with 10% fetal bovine serum (Atlanta Biological, Norcross, GA) and penicillin-streptomycin (Mediatech); Caco-2 medium was further supplemented with nonessential amino acids (Mediatech) and 10 mM 4-(2-hydroxyethyl)-1-piperazineethanesulfonic acid (HEPES; Mediatech), pH 7.4; cells were subcultured every 4–5 d. Human primary dermal fibroblast cells were purchased from ATCC and cultured according their guidelines in fibroblast basal medium (PCS-201-030; ATCC) supplemented with fibroblast growth factor, L-glutamine, ascorbic acid, hydrocortisone, insulin (ATCC), and 2% fetal bovine serum (Sigma-Aldrich, St. Louis, MO). siRNA targeting Caco-2 ZO-1 (Silencer select s14155; Life Technologies, Frederick, MD) or nonspecific siRNA (4390843) was transfected into subconfluent cells cultured on collagen-coated coverslips using RNAiMAX (Life Technologies) transfection reagent and processed for immunofluorescence analysis 72 h posttransfection. Transient transfection of MDCK cells with GFP-labeled constructs was performed in cells plated on glass coverslips or for live-cell imaging on double-chambered glass-bottomed tissue culture wells (Lab-Tek II, Campbell, CA) using Lipofectamine 2000 (Life Technologies) according to the manufacturer's directions; cells were imaged or processed for immunofluorescence 48–96 h posttransfection. Stable knockout cell lines were made by transfecting pSpCas9(BB)-2A-Puro (PX459) V2.0 (62988; Addgene, Cambridge, MA; Ran *et al.*, 2013) using Lipofectamine 2000. Individual clones were isolated after initial selection for 48 h in 2 µg/ml puromycin (Life Technologies), followed by dilution cloning to single cells into 96-well plates. Clonal lines were expanded and tested 2–3 wk after transfection by immunoblot.

HEK293 cells (Tet-off advanced; Clontech, Mountain View, CA) were maintained in high-glucose DMEM supplemented with 10% Tet-qualified fetal bovine serum (Atlanta Biologicals) and penicillin-streptomycin. FuGENE transfection reagent (Promega, Madison, WI) was used for transfection of GFP- and myc-tagged constructs according to the manufacturer's instructions; cells were collected 48 h after transfection and samples processed for immunoprecipitation experiments as described later.

MDCK II Tet-off cells knocked down for ZO-1 and ZO-2 expression have been previously described (Fanning *et al.*, 2012).

DNA constructs

Sequences for all oligonucleotide primers used for cloning and PCR are shown in Supplemental Table S1. GFP-ZO-1 has been previously described (Fanning *et al.*, 2012). A plasmid encoding myc-tagged

TOCA-1 (plasmid 33030; Addgene; Ho *et al.*, 2004) was transferred by infusion cloning into the *Hin*dIII/*Bam*HI sites in pEGFP-C1 (BD Biosciences, San Jose, CA) and PDZ-binding motif added at the same time; this construct is referred to as GFP TOCA-1(+). To make GFP TOCA-1(–), site-directed mutagenesis was used to replace the C-terminal AVTYI PDZ-binding motif with –GS. The coding region of TOCA-1(+) was subcloned into mApple (C1) using *Bam*HI and *Hin*dIII sites. SH3-binding-site mutations W518K in GFP and mApple TOCA-1(+) were generated by site-directed mutagenesis using the same sequences described by Bu *et al.* (2009). Monomeric red fluorescent protein–TOCA-1(–) was kindly provided by Andrew Craig (Queen's University, Kingston, Canada). Myc-tagged TOCA-1(+) was cloned with infusion primers back into the *Eco*RI/*Kpn*I sites of the original pCS+MT vector. GFP FBP17 was obtained from Addgene (plasmid 22229; Itoh *et al.*, 2005).

Stable knockout clones were made using the CRISPR-Cas9 system (Ran *et al.*, 2013); two separate vectors targeting different exons were designed for each TOCA-1 and FBP17. Oligonucleotides were phosphorylated, annealed, and cloned into the *Bbs*I site of pSpCas9(BB)-2A-Puro vector (62988; Addgene) according to the Zhang laboratory protocols (F. Zhang, MIT, Cambridge, MA). All constructs were verified by sequencing. After cloning, DNA was isolated from knockout cell lines and mutations verified by PCR using primers upstream and downstream of the putative mutation sites. GFP-occludin was made by subcloning human occludin (Medina *et al.*, 2000) from pTRE into pTOPO1 and then EGFP C2 with *Hin*dIII. ZO-1 constructs were as previously described (Rodgers *et al.*, 2013); mApple C1 and mEmerald-E-cadherin were gifts from Michael Davidson (Florida State University, Tallahassee, FL).

Antibodies

Mouse anti–ZO-1 (33-9100), claudin-2 (32-5600), and rabbit ZO-2 (38-9100) antibodies were from Life Technologies; rabbit anti-TOCA antibodies were from Bethyl Laboratories (Montgomery, TX; A303-470A) and Millipore (Billerica, MA; ABS70); rabbit anti–N-WASP (30D10), rabbit WAVE2 (D2C8), myosin light chain-S19P (3671P), and mouse Myc-Tag (9B11) antibodies were from Cell Signaling Technology (Beverly, MA); rabbit anti-WIPF2 antibody (HPA024467), rat E-cadherin (U3254), mouse anti–α-actinin, mouse anti–γ-tubulin, and rabbit anti–β-catenin (C2206) were from Sigma Life Science (St. Louis, MO); rabbit anti-Tuba (A303-074A) and FBP17 (A302-790A) antibodies were from Bethyl Laboratories; rabbit anti–myosin 2B (PRB-445P) antibody was from Covance (Madison, WI); rabbit anti-GFP antibody (Ab290) was from Abcam (Cambridge, MA); mouse anti-actin antibody (MAB1501R) was from Millipore; mouse anti–E-cadherin (610181) was from BD Transduction Laboratories (San Jose, CA); mouse anti-CIP4 (sc-135868) was from Santa Cruz Biotechnology (Santa Cruz, CA); and mouse anti-occludin antibody was a generous gift of Jerrold Turner (University of Chicago, Chicago, IL). Antibodies were validated by recognizing bands of the predicted size on immunoblots and by immunolocalization where reported. Antibodies to TOCA-1 and FBP17 were validated by loss of signal in knockout cells. Species-specific secondary antibodies for immunofluorescence (Cy2, Cy3, and Cy5 conjugated) and immunoblots (IR-labeled 680 and 790/800 antibodies) were from Jackson ImmunoResearch (West Grove, PA). Rhodamine–phalloidin was from Life Technologies.

Immunofluorescence microscopy

MDCK and Caco-2 cells were cultured on uncoated or collagen-coated glass coverslips or on Transwell filters (Corning, Corning, NY), fixed in 1% paraformaldehyde in CSK buffer (10 mM 1,4-piperazinediethanesulfonic acid, pH 6.8, 100 mM KCl, 300 mM sucrose, 2 mM $MgCl_2$, and 2 mM ethylene glycol tetraacetic acid) at room temperature for 20 min, permeabilized with 1% Triton X-100 for 10 min, quenched with 50 mM NH_4Cl, and incubated in 2% normal goat serum in phosphate-buffered saline (PBS) for 60 min and in primary antibodies for 60 min. After washing, samples were incubated with fluorescence-labeled secondary antibodies; in some cases rhodamine or Alexa Fluor 647–phalloidin was added with the secondary antibodies. In some cases, cells were fixed with 100% cold ethanol, washed twice with Dulbecco's PBS, and blocked and incubated in primary and secondary antibodies as described. After washing, samples were mounted with Mowiol (EMD, Billerica, MA) containing 1% *n*-propyl gallate (Sigma-Aldrich). Frozen tissue sections from mouse kidney were obtained from the National Heart, Lung, and Blood Institute Pathology Core; animal procedures were carried out in accordance with the guidelines of the National Heart, Lung, and Blood Institute Animal Care and Use Committee. Tissue sections were fixed in 1% paraformaldehyde and immunofluorescence procedures carried out as described. Fixed samples were imaged on a Zeiss (Thornwood, NY) 710 confocal microscope, using either 20×/numerical aperture (NA) 0.8 air or 63×/NA 1.4 oil objectives, with 488-, 561-, and 633-nm laser lines.

Live samples were imaged using a Zeiss 780 confocal microscope using a 63×/1.4 NA lens and heated stage in 5% CO_2; for live-cell imaging, normal medium was supplemented with 20 mM HEPES, pH 7.4. Imaging in dual chambers was of MDCK controls matched with knockout cell lines, each transfected with the same GFP construct; in most cases, GFP–ZO-1 was used. Transfected cells that were in the middle of medium- or large-sized islands were chosen for imaging. Full-section *z*-stacks were imaged at 12 positions (six control, six knockout) every 4 min for 12 h; images were acquired and maximum intensity projections made using Zen 2009. Time-lapse movies were viewed in ImageJ (National Institutes of Health, Bethesda, MD) and cell membrane traces made using the ImageJ plug-in QuimP11b (R. Tyson and T. Bretschneider, Warwick University, Coventry, United Kingdom; warwick.ac.uk/fac/sci/systemsbiology/staff/bretschneider/quimp/). For time-lapse imaging of Arp2/3 inhibition, cells were treated with vehicle (dimethyl sulfoxide [DMSO]) or CK666 (100 μM; Sigma-Aldrich) overnight.

FRAP was performed on a Nikon (Melville, NY) A1R with 63×/NA 1.4 oil objective; bleaching of GFP signal was done with the 405-nm laser line (100% power) in a defined region of interest. Subsequent images were taken at the same focal plane to monitor recovery of fluorescence; images were analyzed using Nikon Elements software; intensity measurements from flanking unbleached membrane regions were used as controls for background intensity changes with time. Subsequent analyses of recovery kinetics were performed using GraphPad Prism.

Laser scission was performed using a Leica (Buffalo Grove, IL) SP5 Multi-Photon (dual beam with OPO)/ Confocal Microscope; images were obtained using a 63×/1.2 NA water immersion lens. Pinhole was adjusted to 3 Airy units and ablation (modified from Verma *et al.*, 2012) performed using a pulsed, femtosecond Ti-sapphire laser (Chameleon; Coherent Scientific, Santa Clara, CA) tuned to 790 nm for 10 m with transmission and gain each set to 60%. GFP fluorescence was detected using a 488-nm laser before and at four 15-s intervals after ablation. The distance between adjacent vertices was measured before and after ablation and the preablation measurement subtracted from the postablation measurements. Values presented are from two independent experiments; $n = 34$ for MDCK control cells and 24 for TOCA-1–knockout cells. Statistical analysis (*t* tests) was performed using Prism with corrections for multiple comparisons using the Sidak–Bonferroni method.

Superresolution images were taken using a GE (Pittsburgh, PA) OMX Blaze V4 Ultrafast Structured Illumination Microscope equipped with four sCMOS cameras using a 60×/1.42 NA lens using 488- and 561-nm laser lines; images were acquired using DeltaVision OMX software; images are projections of slices (~40) over a 3- to 5-µm depth centered on ZO-1 or TOCA-1.

Contrast and colors were adjusted and figures made using Photoshop (Adobe Systems, San Jose, CA) CS5.

Transmission electron microscopy

Cells were grown in 35-mm dishes postconfluence, then directly fixed in 2.5% glutraldehyde and 1% paraformaldehyde in 0.12 M sodium cacodylate buffer, pH 7.4, for 20 min at room temperature and 40 min at 4°C. Cells were postfixed with 1% osmium tetroxide, stained en bloc with uranyl acetate, ethanol dehydrated, and LX112 embedded. Chemicals were from Electron Microscopy Sciences (Hatfield, PA) and Ladd Research Industries. Thin cross sections (70 nm) were cut, stained with uranyl acetate and lead citrate, and viewed with a JEM1400 electron microscope (JEOL USA, Peabody, MA) equipped with an AMT XR-111 digital camera (Advanced Microscopy Techniques Corporation, Woburn, MA).

Freeze-fracture replicas

MDCK cells were fixed in 2% glutaraldehyde in PBS for 1 h, washed, and gradually equilibrated to 30% glycerol as cryoprotectant. The cells were lifted with a cell scraper and rapidly frozen by contact with a polished gold block cooled to −186°C using a LifeCell (Bridgewater, NJ) CF-100 device. Freeze fracture of the samples was performed with a Balzers (Balzers, Liechtenstein) freeze fracture/etch apparatus at −110°C, and samples were unidirectionally shadowed at 45° with platinum and stabilized with carbon deposited from 90°. Replicas were cleaned with sodium hypochlorite and collected onto copper TEM grids. Transmission electron microscopy of the replicas was performed using a JEOL 2100 TEM operating at 200 kV with an Orius 832 camera (Gatan, Pleasanton, CA). Data collection and analysis were performed using the SerialEM/Etomo software suite (Mastronarde, 2005). Average strand number was defined as the number of strands across the tight junction at every 500-nm interval; $n = 40$; five pairs of cells were used for each wild type and knockout.

Pull-down assays and immunoblotting

To test interactions between TOCA-1 and ZO-1 and PDZ-domain deletion constructs, HEK293 Tet-off cells were transfected with inducible myc-tagged ZO-1 N-terminal constructs (amino acids 1–887) containing all three PDZ domains and the N-terminal constructs with the first, second, or third PDZ domains deleted (Rodgers *et al.*, 2013). A second set of HEK cells was transfected with GFP alone, GFP TOCA-1(–), and GFP TOCA-1(+). Cells expressing GFP-labeled constructs were lysed as described and bound to GFP-Trap beads (ChromoTek, Hauppauge, NY) for 60 min at 4°C; beads were washed and then incubated overnight at 4°C with cell lysates from ZO-1–expressing cells as indicated. Beads were washed four times as described, and proteins were eluted with SDS sample buffer and subjected to SDS–gel electrophoresis, transfer, and immunoblot as described.

Quantitative real-time PCR

RNA from confluent 100-mm dishes of Caco-2, MDCK II, and HEK cells and primary dermal fibroblasts were isolated using the RNeasy minikit (Qiagen, Germantown, MD). For qRT-PCR, cDNA was made using Superscript VILO Master Mix (Life Technologies) and PCR carried out with Power Sybr Green Master Mix (Life Technologies). Primers for qRT-PCR are as described in Supplemental Table S1. qRT-PCR was performed using a QuantStudio 7 Flex Real-Time PCR (Life Technologies); levels of TOCA-1(+/–) and FBP17(+/–) are reported relative to ZO-1 values.

Calcium switch and transmonolayer barrier assays

Calcium switch was performed on confluent, polarized MDCK cells (7 d) cultured on Transwell filters; wells were washed with calcium-free medium and changed into S-MEM (Sigma-Aldrich) supplemented with 5% dialyzed fetal bovine serum and penicillin-streptomycin. After overnight incubation, cells were changed back into normal medium; TER (WPI, Sarasota, FL) was measured at the indicated times and filters removed for immunofluorescence analysis. Junction length was measured in ImageJ using the fluorescence signal for ZO-1. Flux assays were carried out as previously described (Van Itallie *et al.*, 2010) using fluorescein-labeled 3-kDa dextran (Life Technologies). Where indicated, cells were pretreated treated with vehicle (DMSO) or the Arp2/3 inhibitor CK666 (100 µM; Sigma-Aldrich) for 30 min and then through the period of the flux assay.

Statistical analyses

All comparisons with three or more conditions were compared by one-way analysis of variance followed by Tukey's or Dunnett's tests. Comparison of two conditions were performed using Student's *t* test. $p < 0.05$ was set as the level for significant difference between groups. Statistics was performed using GraphPad Prism 6 (La Jolla, CA).

ACKNOWLEDGMENTS

We acknowledge Joan Lunney and Sam Abrams (U.S. Department of Agriculture, Beltsville, MD) for help with qRT-PCR and use of their ABI 7500, and Haiming Cao (National Heart, Lung, and Blood Institute, National Institutes of Health, Bethesda, MD) for use of his QuantStudio 7 Flex Real-Time PCR. We thank Xufeng Wu, Daniela Malide, and Christian Combs (Light Microscopy Core Facility, National Heart, Lung, and Blood Institute) and Patricia Connelly, Erin Stempinski, and Chris Brantner (Electron Microscopy Core Facility, National Heart, Lung, and Blood Institute) for their invaluable help and Mary Anne Conti and the National Heart, Lung, and Blood Institute Pathology Core Facility for mouse kidney frozen tissue sections. We appreciate TOCA-1 cDNAs supplied by Andrew Craig (Queen's University, Kingston, Canada) and Sohail Ahmed (Institute of Medical Biology, Singapore). We also thank Alan Fanning (University of North Carolina, Chapel Hill, NC), Karin Fredriksson, and members of the Clare Waterman laboratory, especially Robert Fischer, Ana Pasapera, and Michelle Baird (National Heart, Lung, and Blood Institute), for thoughtful discussions. This research was supported by the Division of Intramural Research, National Institutes of Health.

REFERENCES

Abu Taha A, Taha M, Seebach J, Schnittler HJ (2014). ARP2/3-mediated junction-associated lamellipodia control VE-cadherin-based cell junction dynamics and maintain monolayer integrity. Mol Biol Cell 25, 245–256.

Anderson JM, Van Itallie CM (2009). Physiology and function of the tight junction. Cold Spring Harb Perspect Biol 1, a002584.

Aspenstrom P (1997). A Cdc42 target protein with homology to the non-kinase domain of FER has a potential role in regulating the actin cytoskeleton. Curr Biol 7, 479–487.

Balda MS, Whitney JA, Flores C, Gonzalez S, Cereijido M, Matter K (1996). Functional dissociation of paracellular permeability and transepithelial

electrical resistance and disruption of the apical-basolateral intramembrane diffusion barrier by expression of a mutant tight junction membrane protein. J Cell Biol 134, 1031–1049.
Bentzel CJ, Hainau B, Ho S, Hui SW, Edelman A, Anagnostopoulos T, Benedetti EL (1980). Cytoplasmic regulation of tight-junction permeability: effect of plant cytokinins. Am J Physiol 239, C75–C89.
Bu W, Chou AM, Lim KB, Sudhaharan T, Ahmed S (2009). The Toca-1-N-WASP complex links filopodial formation to endocytosis. J Biol Chem 284, 11622–11636.
Bu W, Lim KB, Yu YH, Chou AM, Sudhaharan T, Ahmed S (2010). Cdc42 interaction with N-WASP and Toca-1 regulates membrane tubulation, vesicle formation and vesicle motility: implications for endocytosis. PLoS One 5, e12153.
Buschmann MM, Shen L, Rajapakse H, Raleigh DR, Wang Y, Lingaraju A, Zha J, Abbott E, McAuley EM, Breskin LA, *et al.* (2013). Occludin OCEL-domain interactions are required for maintenance and regulation of the tight junction barrier to macromolecular flux. Mol Biol Cell 24, 3056–3068.
Chander H, Brien CD, Truesdell P, Watt K, Meens J, Schick C, Germain D, Craig A (2014). Toca-1 is suppressed by p53 to limit breast cancer cell invasion and tumor metastasis. Breast Cancer Res 16, 3413.
Chander H, Truesdell P, Meens J, Craig AW (2013). Transducer of Cdc42-dependent actin assembly promotes breast cancer invasion and metastasis. Oncogene 32, 3080–3090.
Chen VC, Li X, Perreault H, Nagy JI (2006). Interaction of zonula occludens-1 (ZO-1) with alpha-actinin-4: application of functional proteomics for identification of PDZ domain-associated proteins. J Proteome Res 5, 2123–2134.
Chhabra ES, Higgs HN (2007). The many faces of actin: matching assembly factors with cellular structures. Nat Cell Biol 9, 1110–1121.
Clayburgh DR, Barrett TA, Tang Y, Meddings JB, Van Eldik LJ, Watterson DM, Clarke LL, Mrsny RJ, Turner JR (2005). Epithelial myosin light chain kinase-dependent barrier dysfunction mediates T cell activation-induced diarrhea in vivo. J Clin Invest 115, 2702–2715.
Cordenonsi M, D'Atri F, Hammar E, Parry DA, Kendrick-Jones J, Shore D, Citi S (1999). Cingulin contains globular and coiled-coil domains and interacts with ZO-1, ZO-2, ZO-3, and myosin. J Cell Biol 147, 1569–1582.
Cunningham KE, Turner JR (2012). Myosin light chain kinase: pulling the strings of epithelial tight junction function. Ann NY Acad Sci 1258, 34–42.
Etournay R, Zwaenepoel I, Perfettini I, Legrain P, Petit C, El-Amraoui A (2007). Shroom2, a myosin-VIIa- and actin-binding protein, directly interacts with ZO-1 at tight junctions. J Cell Sci 120, 2838–2850.
Fanning AS, Anderson JM (2009). Zonula occludens-1 and -2 are cytosolic scaffolds that regulate the assembly of cellular junctions. Ann NY Acad Sci 1165, 113–120.
Fanning AS, Jameson BJ, Jesaitis LA, Anderson JM (1998). The tight junction protein ZO-1 establishes a link between the transmembrane protein occludin and the actin cytoskeleton. J Biol Chem 273, 29745–29753.
Fanning AS, Van Itallie CM, Anderson JM (2012). Zonula occludens-1 and -2 regulate apical cell structure and the zonula adherens cytoskeleton in polarized epithelia. Mol Biol Cell 23, 577–590.
Fredriksson K, Van Itallie CM, Aponte A, Gucek M, Tietgens AJ, Anderson JM (2015). Proteomic analysis of proteins surrounding occludin and claudin-4 reveals their proximity to signaling and trafficking networks. PLoS One 10, e0117074.
Fricke R, Gohl C, Bogdan S (2010). The F-BAR protein family Actin' on the membrane. Commun Integr Biol 3, 89–94.
Fricke R, Gohl C, Dharmalingam E, Grevelhorster A, Zahedi B, Harden N, Kessels M, Qualmann B, Bogdan S (2009). Drosophila Cip4/Toca-1 integrates membrane trafficking and actin dynamics through WASP and SCAR/WAVE. Curr Biol 19, 1429–1437.
Frost A, Perera R, Roux A, Spasov K, Destaing O, Egelman EH, De Camilli P, Unger VM (2008). Structural basis of membrane invagination by F-BAR domains. Cell 132, 807–817.
Furuse M (2010). Molecular basis of the core structure of tight junctions. Cold Spring Harb Perspect Biol 2, a002907.
Giuliani C, Troglio F, Bai Z, Patel FB, Zucconi A, Malabarba MG, Disanza A, Stradal TB, Cassata G, Confalonieri S, *et al.* (2009). Requirements for F-BAR proteins TOCA-1 and TOCA-2 in actin dynamics and membrane trafficking during Caenorhabditis elegans oocyte growth and embryonic epidermal morphogenesis. PLoS Genet 5, e1000675.
Goldblum SE, Rai U, Tripathi A, Thakar M, De Leo L, Di Toro N, Not T, Ramachandran R, Puche AC, Hollenberg MD, Fasano A (2011). The active Zot domain (aa 288–293) increases ZO-1 and myosin 1C serine/threonine phosphorylation, alters interaction between ZO-1 and its binding partners, and induces tight junction disassembly through proteinase activated receptor 2 activation. FASEB J 25, 144–158.
Gonzalez-Mariscal L, Chavez de Ramirez B, Cereijido M (1985). Tight junction formation in cultured epithelial cells (MDCK). J Membr Biol 86, 113–125.
Guillot C, Lecuit T (2013). Mechanics of epithelial tissue homeostasis and morphogenesis. Science 340, 1185–1189.
Gunzel D, Yu AS (2013). Claudins and the modulation of tight junction permeability. Physiol Rev 93, 525–569.
Han SP, Gambin Y, Gomez GA, Verma S, Giles N, Michael M, Wu SK, Guo Z, Johnston W, Sierecki E, *et al.* (2014). Cortactin scaffolds Arp2/3 and WAVE2 at the epithelial zonula adherens. J Biol Chem 289, 7764–7775.
Heath RJ, Insall RH (2008). F-BAR domains: multifunctional regulators of membrane curvature. J Cell Sci 121, 1951–1954.
Henne WM, Kent HM, Ford MG, Hegde BG, Daumke O, Butler PJ, Mittal R, Langen R, Evans PR, McMahon HT (2007). Structure and analysis of FCHo2 F-BAR domain: a dimerizing and membrane recruitment module that effects membrane curvature. Structure 15, 839–852.
Hetrick B, Han MS, Helgeson LA, Nolen BJ (2013). Small molecules CK-666 and CK-869 inhibit actin-related protein 2/3 complex by blocking an activating conformational change. Chem Biol 20, 701–712.
Hirokawa N, Keller TC 3rd, Chasan R, Mooseker MS (1983). Mechanism of brush border contractility studied by the quick-freeze, deep-etch method. J Cell Biol 96, 1325–1336.
Hirokawa N, Tilney LG (1982). Interactions between actin filaments and between actin filaments and membranes in quick-frozen and deeply etched hair cells of the chick ear. J Cell Biol 95, 249–261.
Ho HY, Rohatgi R, Lebensohn AM, Le M, Li J, Gygi SP, Kirschner MW (2004). Toca-1 mediates Cdc42-dependent actin nucleation by activating the N-WASP-WIP complex. Cell 118, 203–216.
Hu J, Mukhopadhyay A, Craig AW (2011). Transducer of Cdc42-dependent actin assembly promotes epidermal growth factor-induced cell motility and invasiveness. J Biol Chem 286, 2261–2272.
Huo L, Wen W, Wang R, Kam C, Xia J, Feng W, Zhang M (2011). Cdc42-dependent formation of the ZO-1/MRCKbeta complex at the leading edge controls cell migration. EMBO J 30, 665–678.
Itoh T, Erdmann KS, Roux A, Habermann B, Werner H, De Camilli P (2005). Dynamin and the actin cytoskeleton cooperatively regulate plasma membrane invagination by BAR and F-BAR proteins. Dev Cell 9, 791–804.
Ivanov AI, Hunt D, Utech M, Nusrat A, Parkos CA (2005). Differential roles for actin polymerization and a myosin II motor in assembly of the epithelial apical junctional complex. Mol Biol Cell 16, 2636–2650.
Kakimoto T, Katoh H, Negishi M (2006). Regulation of neuronal morphology by Toca-1, an F-BAR/EFC protein that induces plasma membrane invagination. J Biol Chem 281, 29042–29053.
Kamioka Y, Fukuhara S, Sawa H, Nagashima K, Masuda M, Matsuda M, Mochizuki N (2004). A novel dynamin-associating molecule, formin-binding protein 17, induces tubular membrane invaginations and participates in endocytosis. J Biol Chem 279, 40091–40099.
Kovacs EM, Verma S, Ali RG, Ratheesh A, Hamilton NA, Akhmanova A, Yap AS (2011). N-WASP regulates the epithelial junctional actin cytoskeleton through a non-canonical post-nucleation pathway. Nat Cell Biol 13, 934–943.
Kremerskothen J, Stolting M, Wiesner C, Korb-Pap A, van Vliet V, Linder S, Huber TB, Rottiers P, Reuzeau E, Genot E, Pavenstadt H (2011). Zona occludens proteins modulate podosome formation and function. FASEB J 25, 505–514.
Leibfried A, Fricke R, Morgan MJ, Bogdan S, Bellaiche Y (2008). Drosophila Cip4 and WASp define a branch of the Cdc42-Par6-aPKC pathway regulating E-cadherin endocytosis. Curr Biol 18, 1639–1648.
Ma TY, Hollander D, Tran LT, Nguyen D, Hoa N, Bhalla D (1995). Cytoskeletal regulation of Caco-2 intestinal monolayer paracellular permeability. J Cell Physiol 164, 533–545.
Madara JL, Barenberg D, Carlson S (1986). Effects of cytochalasin D on occluding junctions of intestinal absorptive cells: further evidence that the cytoskeleton may influence paracellular permeability and junctional charge selectivity. J Cell Biol 102, 2125–2136.
Madara JL, Stafford J, Dharmsathaphorn K, Carlson S (1987). Structural analysis of a human intestinal epithelial cell line. Gastroenterology 92, 1133–1145.
Marchiando AM, Shen L, Graham WV, Weber CR, Schwarz BT, Austin JR 2nd, Raleigh DR, Guan Y, Watson AJ, Montrose MH, Turner JR (2010). Caveolin-1-dependent occludin endocytosis is required for TNF-induced tight junction regulation in vivo. J Cell Biol 189, 111–126.

Martinez-Quiles N, Rohatgi R, Anton IM, Medina M, Saville SP, Miki H, Yamaguchi H, Takenawa T, Hartwig JH, Geha RS, Ramesh N (2001). WIP regulates N-WASP-mediated actin polymerization and filopodium formation. Nat Cell Biol 3, 484–491.
Mastronarde DN (2005). Automated electron microscope tomography using robust prediction of specimen movements. J Struct Biol 152, 36–51.
Mattagajasingh SN, Huang SC, Hartenstein JS, Benz EJ Jr (2000). Characterization of the interaction between protein 4.1R and ZO-2. A possible link between the tight junction and the actin cytoskeleton. J Biol Chem 275, 30573–30585.
Medina R, Rahner C, Mitic LL, Anderson JM, Van Itallie CM (2000). Occludin localization at the tight junction requires the second extracellular loop. J Membr Biol 178, 235–247.
Mooren OL, Galletta BJ, Cooper JA (2012). Roles for actin assembly in endocytosis. Annu Rev Biochem 81, 661–686.
Nusrat A, Parkos CA, Verkade P, Foley CS, Liang TW, Innis-Whitehouse W, Eastburn KK, Madara JL (2000). Tight junctions are membrane microdomains. J Cell Sci 113, 1771–1781.
Ooshio T, Kobayashi R, Ikeda W, Miyata M, Fukumoto Y, Matsuzawa N, Ogita H, Takai Y (2010). Involvement of the interaction of afadin with ZO-1 in the formation of tight junctions in Madin-Darby canine kidney cells. J Biol Chem 285, 5003–5012.
Otani T, Ichii T, Aono S, Takeichi M (2006). Cdc42 GEF Tuba regulates the junctional configuration of simple epithelial cells. J Cell Biol 175, 135–146.
Pulimeno P, Paschoud S, Citi S (2011). A role for ZO-1 and PLEKHA7 in recruiting paracingulin to tight and adherens junctions of epithelial cells. J Biol Chem 286, 16743–16750.
Ran FA, Hsu PD, Wright J, Agarwala V, Scott DA, Zhang F (2013). Genome engineering using the CRISPR-Cas9 system. Nat Protoc 8, 2281–2308.
Rodgers LS, Beam MT, Anderson JM, Fanning AS (2013). Epithelial barrier assembly requires coordinated activity of multiple domains of the tight junction protein ZO-1. J Cell Sci 126, 1565–1575.
Rodgers LS, Fanning AS (2011). Regulation of epithelial permeability by the actin cytoskeleton. Cytoskeleton (Hoboken) 68, 653–660.
Rohatgi R, Ma L, Miki H, Lopez M, Kirchhausen T, Takenawa T, Kirschner MW (1999). The interaction between N-WASP and the Arp2/3 complex links Cdc42-dependent signals to actin assembly. Cell 97, 221–231.
Rolland Y, Marighetti P, Malinverno C, Confalonieri S, Luise C, Ducano N, Palamidessi A, Bisi S, Kajiho H, Troglio F, *et al.* (2014). The CDC42-interacting protein 4 controls epithelial cell cohesion and tumor dissemination. Dev Cell 30, 553–568.
Rotty JD, Wu C, Bear JE (2013). New insights into the regulation and cellular functions of the ARP2/3 complex. Nat Rev Mol Cell Biol 14, 7–12.
Roux KJ, Kim DI, Raida M, Burke B (2012). A promiscuous biotin ligase fusion protein identifies proximal and interacting proteins in mammalian cells. J Cell Biol 196, 801–810.
Sawyer JM, Harrell JR, Shemer G, Sullivan-Brown J, Roh-Johnson M, Goldstein B (2010). Apical constriction: a cell shape change that can drive morphogenesis. Dev Biol 341, 5–19.
Shen L, Weber CR, Raleigh DR, Yu D, Turner JR (2011). Tight junction pore and leak pathways: a dynamic duo. Annu Rev Physiol 73, 283–309.
Shimada A, Niwa H, Tsujita K, Suetsugu S, Nitta K, Hanawa-Suetsugu K, Akasaka R, Nishino Y, Toyama M, Chen L, *et al.* (2007). Curved EFC/F-BAR-domain dimers are joined end to end into a filament for membrane invagination in endocytosis. Cell 129, 761–772.
Songyang Z, Fanning AS, Fu C, Xu J, Marfatia SM, Chishti AH, Crompton A, Chan AC, Anderson JM, Cantley LC (1997). Recognition of unique carboxyl-terminal motifs by distinct PDZ domains. Science 275, 73–77.
Takano K, Toyooka K, Suetsugu S (2008). EFC/F-BAR proteins and the N-WASP-WIP complex induce membrane curvature-dependent actin polymerization. EMBO J 27, 2817–2828.
Timpe L, Martz E, Steinberg MS (1978). Cell movements in a confluent monolayer are not caused by gaps: evidence for direct contact inhibition of overlapping. J Cell Sci 30, 293–304.
Tsujita K, Suetsugu S, Sasaki N, Furutani M, Oikawa T, Takenawa T (2006). Coordination between the actin cytoskeleton and membrane deformation by a novel membrane tubulation domain of PCH proteins is involved in endocytosis. J Cell Biol 172, 269–279.
Tyson RA, Zatulovskiy E, Kay RR, Bretschneider T (2014). How blebs and pseudopods cooperate during chemotaxis. Proc Natl Acad Sci USA 111, 11703–11708.
Van Itallie CM, Anderson JM (2006). Claudins and epithelial paracellular transport. Annu Rev Physiol 68, 403–429.
Van Itallie CM, Aponte A, Tietgens AJ, Gucek M, Fredriksson K, Anderson JM (2013). The N and C termini of ZO-1 are surrounded by distinct proteins and functional protein networks. J Biol Chem 288, 13775–13788.
Van Itallie CM, Balda MS, Anderson JM (1995). Epidermal growth factor induces tyrosine phosphorylation and reorganization of the tight junction protein ZO-1 in A431 cells. J Cell Sci 108, 1735–1742.
Van Itallie CM, Fanning AS, Holmes J, Anderson JM (2010). Occludin is required for cytokine-induced regulation of tight junction barriers. J Cell Sci 123, 2844–2852.
Verma S, Han SP, Michael M, Gomez GA, Yang Z, Teasdale RD, Ratheesh A, Kovacs EM, Ali RG, Yap AS (2012). A WAVE2-Arp2/3 actin nucleator apparatus supports junctional tension at the epithelial zonula adherens. Mol Biol Cell 23, 4601–4610.
Yan S, Lv Z, Winterhoff M, Wenzl C, Zobel T, Faix J, Bogdan S, Grosshans J (2013). The F-BAR protein Cip4/Toca-1 antagonizes the formin Diaphanous in membrane stabilization and compartmentalization. J Cell Sci 126, 1796–1805.
Zhao H, Michelot A, Koskela EV, Tkach V, Stamou D, Drubin DG, Lappalainen P (2013). Membrane-sculpting BAR domains generate stable lipid microdomains. Cell Rep 4, 1213–1223.
Zhou K, Muroyama A, Underwood J, Leylek R, Ray S, Soderling SH, Lechler T (2013). Actin-related protein2/3 complex regulates tight junctions and terminal differentiation to promote epidermal barrier formation. Proc Natl Acad Sci USA 110, E3820–E3829.
Zobel T, Brinkmann K, Koch N, Schneider K, Seemann E, Fleige A, Qualmann B, Kessels MM, Bogdan S (2015). Cooperative functions of the two F-BAR proteins Cip4 and Nostrin in regulating E-cadherin in epithelial morphogenesis. J Cell Sci 128, 499–515.
Zolotarevsky Y, Hecht G, Koutsouris A, Gonzalez DE, Quan C, Tom J, Mrsny RJ, Turner JR (2002). A membrane-permeant peptide that inhibits MLC kinase restores barrier function in in vitro models of intestinal disease. Gastroenterology 123, 163–172.